Brosens, L., Campforts, B., Robinet, J., Vanacker, V., Opfergelt, S., Ameijeiras-Mariño, Y., Minella, J. P. G., Govers, G. (2020): Slope Gradient Controls Soil Thickness and Chemical Weathering in Subtropical Brazil: Understanding Rates and Timescales of Regional Soilscape Evolution Through a Combination of Field Data and Modeling. - Journal of Geophysical Research: Earth Surface, 125, 6, e2019JF005321.

https://doi.org/10.1029/2019JF005321

JGR Earth Surface

RESEARCH ARTICLE
10.1029/2019JF005321

Key Points:
- Soil thickness and weathering degree decrease with increasing slope gradient
- Combining a numerical model with field data enabled us to constrain soil residence times between ~20 and 1700 kyr, which strongly decrease with increasing slope gradient
- Simulated weathering rates might vary by 2 orders of magnitudes and increase with increasing slope gradient and erosion rate

Supporting Information:
- Supporting Information S1

Correspondence to:
L. Brosens,
liesa.brosens@kuleuven.be

Citation:
Brosens, L., Campforts, B., Robinet, J., Vanacker, V., Opfergelt, S., Ameijeiras-Mariño, Y., et al. (2020). Slope gradient controls soil thickness and chemical weathering in subtropical Brazil: Understanding rates and timescales of regional soilscape evolution through a combination of field data and modeling. *Journal of Geophysical Research: Earth Surface*, *125*, e2019JF005321. https://doi.org/10.1029/2019JF005321

Received 24 AUG 2019
Accepted 17 APR 2020
Accepted article online 26 April 2020

Slope Gradient Controls Soil Thickness and Chemical Weathering in Subtropical Brazil: Understanding Rates and Timescales of Regional Soilscape Evolution Through a Combination of Field Data and Modeling

Liesa Brosens[1,2], Benjamin Campforts[1,3,4], Jérémy Robinet[2], Veerle Vanacker[5], Sophie Opfergelt[6], Yolanda Ameijeiras-Mariño[6], Jean P. G. Minella[7], and Gerard Govers[2]

[1]Research Foundation Flanders (FWO), Brussels, Belgium, [2]Division of Geography and Tourism, Department of Earth and Environmental Sciences, KU Leuven, Leuven, Belgium, [3]Helmholtz Centre Potsdam, GFZ German Research Centre for Geosciences, Potsdam, Germany, [4]Institute for Arctic and Alpine Research, University of Colorado Boulder, Boulder, CO, USA, [5]Earth and Life Institute, Georges Lemaître Centre for Earth and Climate Research, Université Catholique de Louvain, Louvain-la-Neuve, Belgium, [6]Earth and Life Institute, Environmental Sciences, Université Catholique de Louvain, Louvain-la-Neuve, Belgium, [7]Department of Soil, Universidade Federal de Santa Maria, Santa Maria, Brazil

Abstract Soil thickness and residence time are regulated by a dynamic interplay between soil formation and lateral transport of soil particles and solutes. To unravel this interplay and infer patterns and rates of chemical weathering, soil physical and chemical properties can be used. Here, we present an integrated approach combining numerical modeling with field measurements to assess the impact of slope gradient on soil thickness and chemical weathering at a regional scale. We first perform a number of synthetic model runs simulating soil formation, weathering, erosion, and deposition, which show that soil thickness and weathering degree decline with increasing slope gradient. We then evaluate how those functional relationships compare to soil-landscape data observed in the field. Soils are sampled at 100 midslope positions under varying slope gradient. The weathering degree is determined using three chemical weathering indices: ratio of iron oxides to total iron (Fe_d/Fe_t), chemical index of alteration (*CIA*), and total reserve in bases (*TRB*). Finally, we calibrate the Be2D model to our field data to constrain soil residence times and chemical weathering rates. The modeled weathering rates decrease with increasing soil residence time and decreasing slope gradient. The application of the soil-landscape evolution model in Southern Brazil shows that weathering rates can vary up to 2 orders of magnitude and depend on hillslope gradient. Notwithstanding model limitations and data uncertainties, we demonstrate the potential of an integrated approach, where field data and numerical modeling are integrated to unravel the timescale of soil weathering along transport over hillslopes.

Plain Language Summary By combining a numerical soil-landscape evolution model with field data we assess the impact of topography on soil thickness and chemical weathering degrees and rates. Chemical weathering degrees are indicative of the extent of chemical weathering of the soil mantle, whereas weathering rates indicate how fast the chemical composition is changing over time. We show that on steep slopes soils are thinner and have a lower weathering degree compared to gentle slopes. The observed difference in soil weathering is related to the soil residence time, which is constrained by combining field measurements with a numerical model. Soils developed on basalt and dacite-rhyolite rocks in a subtropical climate regime have soil residence times ranging between ~20 and 1700 kyr. Soils on steep slopes are younger and characterized by weathering rates that can be twice as high as for older soils on gentle slopes. Integrating field data in soil-landscape evolution models can help to unravel the interplay between topography, soil erosion, and weathering in soil-mantled landscapes.

1. Introduction

Soils are open systems through which material flows. The balance between soil production and denudation controls soil thickness (Brantley, 2008; Burke et al., 2007; Minasny & McBratney, 2001). Until recently, soil development was mainly studied at the pedon or catena scale in near-level, slowly eroding, landscapes,

where soil production at the saprolite-soil interface and processes inducing vertical exchanges (water flow, bioturbation) dominate (Chorover et al., 2007; Johnson et al., 2014; Lebedeva et al., 2010; Opolot et al., 2015; Rasmussen & Tabor, 2007). In the past two decades, soil processes in eroding landscapes have gained attention (Green et al., 2006; Nezat et al., 2004; Tsui et al., 2004; Wackett et al., 2018; Yoo et al., 2007). In eroding landscapes, topography controls soil erosion, thereby determining soil thickness and residence time of soil particles (e.g., Anderson, 2015; Tucker & Bradley, 2010; Yoo et al., 2007). Lateral fluxes of soil constituents along slope may thus be as—and even more—important than vertical fluxes in explaining spatial variations in soil properties (Jelinski et al., 2019; Molina et al., 2019; Yoo et al., 2007).

Previously reported relationships between slope gradient and soil thickness, weathering degrees and rates at the hillslope scale yield varying results. Negative correlations between soil thickness and slope have been reported by several authors (Florinsky et al., 2002; Gessler et al., 2000; Mehnatkesh et al., 2013; Thompson et al., 2006; Tsai et al., 2001), but there is no unique relationship between both factors. Reaney (2003) derived a linear dependence of soil thickness and slope, in contrast to the power relationship reported earlier by Derose et al. (1993). Similarly, there are no conclusive results on the influence of slope on weathering degree and rate. Recent work has shown decreasing (Burke et al., 2007; Vanacker et al., 2019) and increasing (Osat et al., 2016) weathering degrees with increasing slope gradient. Burke et al. (2007, 2009) and Dixon et al. (2012) reported that chemical weathering rates may both decrease or increase with increasing slope gradient, depending on the geomorphic landscape position of the sites (highland vs. lowland).

Field observations alone generally do not allow to establish causal relationships between spatial variations in soil properties (including soil thickness) and landscape position. This is because they are, as such, insufficient to assess the relative importance of the different processes. Fully understanding the control of slope gradient on soil thickness and chemical weathering degrees and rates requires an approach whereby hillslope position and slope morphology are explicitly accounted for and where both vertical (in situ) and lateral (transport of soil particles and solutes) processes are integrated in a single numerical framework. It then also becomes possible to investigate how sloping soil-covered landscapes evolve over time (Green et al., 2006; Mudd & Furbish, 2006; Wackett et al., 2018; Yoo & Mudd, 2008).

In this study, we explore such an integrated modeling-data approach in order to assess the impact of slope gradient on soil thickness, weathering degrees and rates, and how these can be related to soil residence times. We do so by investigating these relationships at a regional scale in a subtropical soil-covered landscape located on the southern edge of the Brazilian plateau, where Acrisols, Cambisols, and Leptosols have developed on basalt and dacite-rhyolite lithology. In this paper we first discuss the theoretical background of soil production, chemical weathering, and physical erosion, after which we explain how these are incorporated in the enhanced Be2D model developed by Campforts et al. (2016). Subsequently, Be2D is used to simulate the effect of slope gradient on soil thickness and weathering degree and rate and to explore how these variables interact through a series of synthetic model runs. In a next step, we apply the model to explore the relationships between slope gradient, soil thickness, and weathering degree that we observed in the field, whereby we focus on the variations in soil properties at the midslope topographic position. In this way we investigate to what extent model simulations can be used to constrain soil residence times in our study area and establish relationships between soil residence times and weathering degrees and rates along eroding hillslopes.

2. Theoretical Background on Soil Production, Chemical Weathering, and Physical Erosion Models

2.1. Soil Production

The coupling between soil production and soil thickness was first recognized by Gilbert (1877). He suggested that an inverse relationship might exist between soil thickness and soil production: Soil production rates would be slowest in very shallow soils due to their low water-holding capacity, and in deep soils due to slow weathering at deep reaction fronts. The soil production rate was therefore assumed to be highest at an intermediate soil thickness, giving rise to "humped" soil production functions (Humphreys & Wilkinson, 2007; Minasny et al., 2008). Several humped as well as other functional relationships have been proposed by, for example, Cox (1980), Furbish and Fagherazzi (2001), Minasny and McBratney (2006), and Saco et al. (2006).

Soil production rates have now been measured across a wide range of environmental settings, based on cosmogenic ^{10}Be and ^{26}Al concentrations (e.g., Dixon et al., 2009; Heimsath et al., 1997, 1999; Small et al., 1999). Generally, measurements do not support the humped model in soil-mantled landscapes (Humphreys & Wilkinson, 2007): Soil production rates (φ [L T^{-1}]) generally decline exponentially with increasing soil thickness (d [L]):

$$\varphi(t, x) = P_0 e^{-\alpha d(t,x)} \tag{1}$$

where P_0 [L T^{-1}] is the soil production rate of the parent material when the soil thickness equals zero and α [L^{-1}] is the depth scaling factor.

2.2. Chemical Weathering

2.2.1. Weathering Indices

In the remaining part of the paper, we make a clear distinction between weathering degree and weathering rate. The *degree* of soil weathering is the extent of chemical alteration of the soil mantle with respect to the saprolite or bedrock at a given point in time. The weathering *rate* refers to the amount of change in weathering degree over time and corresponds to the mass that is chemically altered or removed per unit of time (Bland & Rolls, 2016). Deriving weathering rates thus requires information on two variables: (i) the degree of weathering and (ii) the time period over which weathering reactions have been taking place, which is often unknown (Green et al., 2006; Mudd & Yoo, 2010).

Since the beginning of the twentieth century more than 30 chemical weathering indices have been proposed, which can be used to assess the weathering degree of soils based on their chemical and/or mineralogical composition (Fiantis et al., 2010). In our multiproxy approach, three of these indices are used: the ratio of iron oxides extracted with dithionite-citrate-bicarbonate (*DCB*) to total iron (Fe_d/Fe_t), the chemical index of alteration (*CIA*), and the total reserve in bases (*TRB*) (details about laboratory procedures can be found in Text S1 in the supporting information). The principal assumption of these indices is that the degree of weathering can be derived from the relative abundance of chemical elements and/or their oxidation state (Ameijeiras-Mariño et al., 2017; Duzgoren-Aydin et al., 2002). As weathering advances, iron in primary minerals is released and becomes oxidized, hence the ratio of oxidized iron (Fe_d) to total iron (Fe_t) increases, ranging between 0 for fresh and 1 for fully weathered material (Buol et al., 2011; Chesworth, 2008; Huang, 2011; Price & Velbel, 2003). The *CIA* (−) reflects the degree of weathering as the proportion of a conservative oxide, Al_2O_3, to the sum of the major oxides (Fedo et al., 1995; Nesbitt & Young, 1982, 1989):

$$CIA = 100\left[\frac{Al_2O_3}{Al_2O_3 + CaO + Na_2O + K_2O}\right] \tag{2}$$

Soils with *CIA* values between 90 and 100 are highly weathered, with depletion of the base cations. The *TRB* ($cmol_c kg^{-1}$) represents the sum of the total amount of alkaline and alkaline-earth elements (Ca^{2+}, K^+, Mg^{2+}, and Na^{2+}). The *TRB* in soils decreases with increasing weathering as soil chemical weathering results in a removal of mobile Ca, K, Mg, and Na cations from the soil matrix (Delvaux et al., 1989; Herbillon, 1986).

$$TRB = Ca^{2+} + Mg^{2+} + K^+ + Na^+ \tag{3}$$

2.2.2. (Extended) Chemical Depletion Fraction

While weathering indices are a useful tool to assess relative differences and changes in weathering degree over time, their values depend on bedrock mineralogy and chemical composition. Geochemical mass balance approaches (Brimhall & Dietrich, 1987) that use conservative elements (inert to chemical weathering), enable to overcome some of these limitations (Riebe et al., 2001, 2003, 2004). The soil chemical depletion fraction (*CDF*) relies on steady state mass balance equations that are valid when the soil production rate (φ) is equal to the denudation rate (D), which is the sum of the physical erosion rate (E) and chemical weathering rate (W), all in L T^{-1}. The *CDF* expresses the fraction of the overall mass loss that is accounted for by chemical losses (Riebe et al., 2003). As conservative elements (such as Nb, Ti, or Zr) are enriched in the soil mantle during chemical weathering, the weathering degree can be determined as the enrichment in concentration (C) of a conservative element (i) in the soil (s) compared to its concentration in the parent material (p):

$$CDF = \frac{W}{\varphi} = \frac{W}{D} = 1 - \frac{C_{i,p}}{C_{i,s}} \quad (4)$$

Hereby, it is assumed that soils are in steady state, where soil transport, production, and chemical weathering are balanced and soil thickness does not change over time. This steady state assumption also implies that the obtained *CDF* values are time averages, where the measured (instantaneous) value equals the mean value. Other assumptions are that soil chemistry and composition do not change over time and that there is no loss of the conservative element in the soil/bedrock system or external inputs (e.g., dust).

On eroding hillslopes, the chemical weathering degree of the soil mantle will depend on weathering processes in the underlying parent material, the lateral soil fluxes, and the weathering degree of the eroded soil from upslope positions. The extended chemical depletion fraction (*ECDF*) as proposed by Yoo et al. (2007) takes into account the effects of physical soil erosion on the chemical depletion of the soil mantle on hillslopes, again assuming steady state conditions:

$$ECDF = CDF + \frac{\nabla C_{i,s}}{C_{i,s}} \cdot \frac{Q_{\text{tot}}}{\phi} \quad (5)$$

The second term on the right-hand side of equation 5 can be seen as the "corrective" term for downslope soil movement along slopes, the magnitude of which is proportional to the ratio of the total lateral soil flux (Q_{tot} [M L^{-1} T^{-1}]) to the local soil production rate (ϕ [M L^{-2} T^{-1}]) and to the ratio of the lateral gradient of the chemically inert element ($\nabla C_{i,s}$ [L^{-1}]) to the concentration of this inert element. The soil production rate ϕ in M L^{-2} T^{-1} is obtained by multiplying φ in L T^{-1} with the soil bulk density ρ_s [M L^{-3}]. As the total soil flux is considered, this implies that *ECDF* is a depth-averaged value and that $C_{i,s}$ is the depth-averaged elemental concentration. Throughout this manuscript the term weathering degree refers to both measured weathering indices (*CIA*, *TRB*, and Fe_d/Fe_t) and modeled *ECDF* values.

2.2.3. Weathering Rates

At steady state, the *CDF* is the chemical weathering rate normalized by the total denudation rate (Riebe et al., 2004, equation 4). Outside steady state, however, the *CDF* as measured at a certain point in time is an indication of the average weathering degree of the soil mantle. While weathering indices and *CDF*/*ECDF* give information on, respectively, the relative and absolute *degree* of soil chemical weathering, they do not quantify the *rate* at which these processes take place. In topographic steady state, average long-term chemical weathering rates are generally determined using mass balance methods, where the rate equals the total mass loss over soil age (e.g., Chadwick et al., 1990; Merritts et al., 1991; White et al., 1996). In steady state, with limited input of soil material from upslope and negligible atmospheric deposits of dust and/or solutes, weathering rates can also be quantified without explicitly calculating soil age by combining the *CDF* with soil production rates (equation 4, Riebe et al., 2001, 2003, 2004). In erosional contexts the input of chemically weathered material from upslope to the soil plays an important role. In this case the soil weathering rate can be constrained by using soil residence time instead of soil age (Anderson et al., 2002; Riebe et al., 2003; White et al., 1998) and by explicitly accounting for mineral supply rates from the underlying saprolite as well as from weathered soil material transported from upslope as proposed by Yoo et al. (2007) (equation 5).

2.3. Soil Erosion

Two main types of soil transport are commonly incorporated in mass balance models: diffusive transport and water erosion (Minasny et al., 2008). Total erosion rates E_{tot} [L T^{-1}]) can then be obtained by taking the sum of the water (E_w [L T^{-1}]) and diffusive (E_d [L T^{-1}]) component:

$$E_{\text{tot}}(t, x) = E_w(t, x) + E_d(t, x) \quad (6)$$

In the most simple model, the diffusive soil flux (Q_d [M $L^{-1}T^{-1}$]) is linearly proportional to the slope gradient (change in height h [L] with distance x [L]) over time t [T]:

$$Q_d(t,\,x) = -\rho_s k \frac{\partial h(t,\,x)}{\partial x} \tag{7}$$

where k[$L^2\ T^{-1}$] is the transport coefficient and ρ_s [$M\ L^{-3}$] the soil bulk density. The flux is calculated in the x direction and per unit width.

When adding a soil thickness term (d [L]) with transport coefficient K [$L\ T^{-1}$], spatial variations in soil thickness are better represented, as it was shown that the linear soil flux-slope gradient relationship is only applicable for convex regions with shallow slope gradients (Heimsath et al., 2005; Pelletier & Rasmussen, 2009; Roering et al., 1999):

$$Q_d(t,\,x) = -\rho_s K d(t,\,x) \frac{\partial h(t,\,x)}{\partial x} \tag{8}$$

Diffusive erosion rates (E_d [$L\ T^{-1}$]) are equal to ∇Q_{d}, which reduces to the derivative of Q_d with respect to x for a one-dimensional hillslope. In a discrete model diffusive soil fluxes (Q_d [$M\ L^{-1}\ T^{-1}$]) are converted to erosion rates [$L\ T^{-1}$] by calculating the difference between influx and outflux ($Q_{d,\mathrm{in}} - Q_{d,\mathrm{out}}$), divided by the product of the horizontal resolution (Δx) and soil bulk density.

Erosion by overland flow (E_w [$M\ L^{-2}T^{-1}$]) can be divided into a rill (E_r [$M\ L^{-2}T^{-1}$]) and interrill (E_{ir} [$M\ L^{-2}T^{-1}$]) erosion component according to the framework developed by Govers et al. (1994). Rill erosion is a power function of slope length (x [L]) and slope gradient ($\frac{\partial h}{\partial x}$ [−]), whereas interrill erosion is a power function of slope alone. g_r and g_{ir} [$L\ T^{-1}$] are, respectively, the rill and inter-rill erosion coefficient, m, m_{ir}, and n [−] the slope and length exponent for (inter-)rill erosion and x_{ref} [L] the reference length (taken as 1 m).

$$E_r(t,\,x) = \rho_s g_r \left(\frac{\partial h(t,x)}{\partial x}\right)^m \left(\frac{x}{x_{\mathrm{ref}}}\right)^n \tag{9}$$

$$\mathrm{E}_{ir}(t,\,x) = \rho_s g_{ir} \left(\frac{\partial h(t,x)}{\partial x}\right)^{m_{ir}} \tag{10}$$

$$g_{ir} = 3.68\ g_r \tag{11}$$

$$E_w(t,\,x) = E_r(t,\,x) + E_{ir}(t,\,x) \tag{12}$$

When the mobilized soil material exceeds the local transport capacity (T_c [$M\ L^{-1}\ T^{-1}$]) sediment is deposited. Govers et al. (1994) related the local transport capacity to the potential rill erosion by the transport capacity coefficient g_t [L]:

$$T_c(t,\,x) = g_t E_w(t,\,x) \tag{13}$$

Water erosion rates (E_w [$M\ L^{-2}\ T^{-1}$]) are converted to rates in $L\ T^{-1}$ and water erosion fluxes (Q_w [$M\ L^{-1}\ T^{-1}$]) in the x direction per unit width by, respectively, dividing by ρ_s and multiplying with Δx. The total erosion flux (Q_{tot} [$M\ L^{-1}\ T^{-1}$]) is then the sum of the diffusive and water flux. The total incoming soil flux at a given location is $Q_{\mathrm{tot,in}}$, the total outgoing flux $Q_{\mathrm{tot,out}}$.

3. Material and Methods

3.1. The Be2D Model

3.1.1. Structure

The steady state soil thickness is constant and determined by the balance between soil production from the underlying saprolite on the one hand and soil removal/addition by physical erosion/deposition and chemical weathering on the other hand (Figure 1):

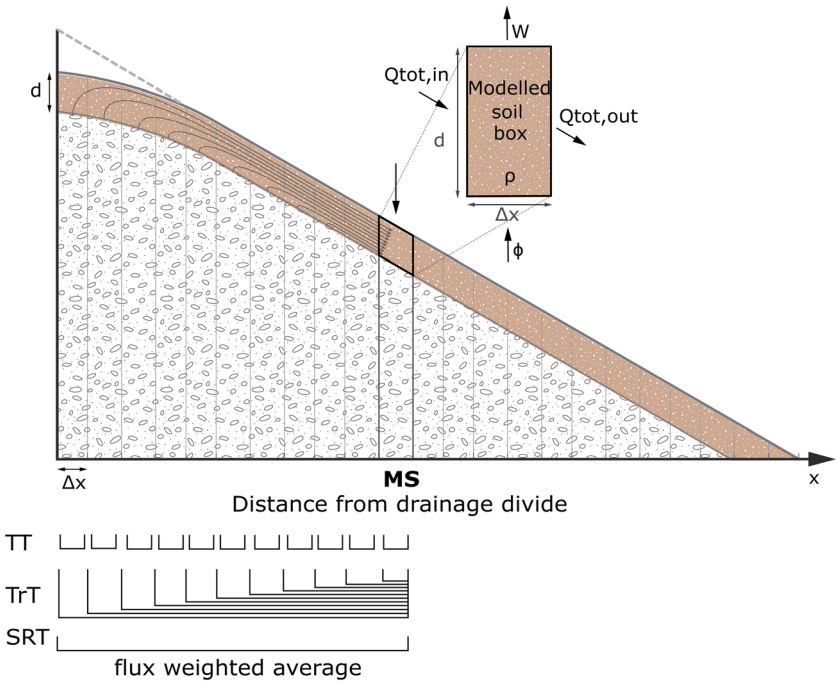

FIGURE 1. Conceptual representation of the soil-landscape evolution model based on Almond et al. (2007). The parallelogram-shaped soil box along slope is discretized as a rectangle shaped box in the numeral model. Soil thickness (d[L]) is determined by the balance between the soil production rate (φ [L T^{-1}]), chemical weathering rate (W [L T^{-1}]), and total physical erosion/deposition rate (E_{tot}[L T^{-1}]), which is equal to the difference in total mass influx and outflux ($Q_{tot,in} - Q_{tot,out}$ [M L^{-1}T^{-1}]) multiplied with soil bulk density ρ_s [M L^{-3}] over Δx [L]. Modeled hillslopes are initially linear all along the hillslope (dashed light gray line), evolving to a convex hilltop (dark gray line) over time. Turnover time (TT[T]) is calculated at each hillslope position x as the time required to remove all the material from the two-dimensional soil box (with thickness d, soil bulk density ρ_s, and horizontal resolution Δx) by the total outflux $Q_{tot,out}$. Particle transit timSs (TrT) at a given hillslope position are calculated as the sum of the TT of all upslope positions, where the soil residence time (SRT[T]) at a given location is the flux-weighted average of these particle transit times. The modeled soil residence time at the sampled midslope (MS) position is used in our analysis and visually represented here.

$$\frac{\partial d(t,x)}{\partial t} = \varphi(t,x) - E_{tot}(t,x) - W(t,x) \tag{14}$$

The domain represented in our model is the soil layer, bounded by the underlying saprolite. We assume soil production to decline exponentially with soil thickness as described by equation 1. The total physical erosion rate consists of both a diffusive and water erosion component. Water erosion is calculated following the framework developed by Govers et al. (1994) as explained in section 2.3 and is modeled by applying equations 9 to 13. The depth-dependent diffusive equation is used (equation 8) in order to calculate diffusive erosion rates.

Chemical weathering rates (W [L T^{-1}]) are calculated by assuming an exponential decrease in weathering rate with increasing soil thickness, similar to the exponential soil production function (equation 1):

$$W(t,x) = W_0 e^{-\beta d(t,x)} \tag{15}$$

where W_0[L T^{-1}] represents the weathering rate of the soil when the soil thickness is zero and β [L^{-1}] the depth scaling factor. This is in agreement with empirical data of Burke et al. (2007, 2009) and Yoo et al. (2009), who demonstrated that chemical weathering rates indeed decrease exponentially with increasing soil thickness. This is commonly attributed to soil water availability and fluid residence times (Rasmussen et al., 2010; Schoonejans et al., 2016). The continuity equation (equation 14) is solved using an explicit first-order finite difference scheme, which is described in more detail in Campforts et al. (2016).

3.1.2. Deriving Soil Residence Times

Calculating soil residence times on eroding landscapes requires taking into account both the mineral supply from the underlying saprolite as well as the input of (weathered) soil material from upslope (Yoo et al., 2007). The turnover time (TT [T]) of a soil box at each hillslope position is the average time a soil particle will reside in the box. The dimensions of the soil box are determined by the horizontal resolution Δx [L] and soil thickness d [L], and the removal of soil is given by the total outflux Q_{tot}[M $\mathrm{L}^{-1}\mathrm{T}^{-1}$] (Yoo et al., 2007, Figure 1):

$$TT(t,\,x)=\frac{\rho_s\,d(t,\,x)\Delta x}{Q_{\mathrm{tot}}(t,\,x)} \tag{16}$$

The soil at a given hillslope position x is composed of particles with a distribution of ages, as it comprises particles derived from in situ bedrock weathering, as well as soil particles eroded from different upslope positions (Almond et al., 2007, Figure 1). The average time needed for a particle to travel from the drainage divide to position x is given by its transit time (TrT [T]):

$$TrT(t,\,x)=\sum_{i=1}^{x}TT_i(t,\,x) \tag{17}$$

As the soil at hillslope position x will be composed of a mix of particles coming from all upslope positions, the soil residence time (SRT [T]) for the soil material at location x can then be calculated as the flux-weighted average of all upslope particle transit times (Almond et al., 2007, Figure 1):

$$SRT(t,\,x)=\frac{\sum_{i=1}^{x}\left(Q_{\mathrm{tot},i}\;TrT_i(t,\,x)\right)}{\sum_{i=1}^{x}Q_{\mathrm{tot},i}(t,\,x)} \tag{18}$$

A more detailed explanation with an example on our SRT calculations is provided in Text S2 and Figure S1.

3.2. Synthetic Model Runs

In the synthetic model runs, we use the $ECDF$ to quantify weathering degree. Here, we model the $ECDF$ by simulating the change in concentration C of an inert element i in the soil ($C_{i,s}$) at each hillslope position over time based on the modeled soil fluxes. We thus model the changes in concentration of the inert element without explicitly modeling mineral conversion (e.g., Ferrier & Kirchner, 2008).

At the beginning of a time step, a soil box at position x has a given mass (m_s) and conservative element concentration ($C_{i,s}$ (t,x)). Soil with different inert elemental concentrations is then added and removed (Figure 1), resulting in a new concentration of the inert element in the soil box ($C_{i,s}$(t+1,x)). This new concentration is calculated by dividing the new mass of the inert element in the box (numerator of equation 19) over the new mass of the soil box (denominator of equation 19). Soil is added to the box from upslope positions ($Q_{\mathrm{tot},in}$) and is produced in situ from the parent material (p) at a rate equal to the soil production rate φ. At the same time soil is leaving the box due to lateral soil movement ($Q_{\mathrm{tot,out}}$) and chemical weathering (W). For conservative elements, there is no significant mass loss via chemical weathering; therefore, chemical weathering is not present in the numerator of equation 19.

$$C_{i,s}(t+1,\,x)=\frac{C_{i,s}(t,\,x)\;m_s+C_{i,p}(t,\,x)\;m_p+C_{i,\mathrm{Qtot,in}}(t,\,x)\;m_{\mathrm{Qtot,in}}-C_{i,\mathrm{Qtot,out}}(t,\,x)\;m_{\mathrm{Qtot,out}}}{m_s+m_p+m_{s,\mathrm{Qtot,in}}-m_{s,\mathrm{Qtot,out}}-m_{s,W}} \tag{19}$$

The new $ECDF$ values can then be calculated using CDF equation 4, as the contribution of lateral processes is already accounted for when calculating the new soil inert element concentration ($C_{i,s}$ (t+1,x)), thereby comprising the second term of equation 5.

$$ECDF(t+1,\,x)=1-\frac{C_{i,p}(t,\,x)}{C_{i,s}(t+1,\,x)} \tag{20}$$

The concentration of the chemically inert element in the saprolite ($C_{i,p}$) is assumed to be constant throughout time and along the hillslope. As weathering rates are the change in weathering degree over time, they can be calculated by taking the derivative of the relationship between the weathering degree (given by the

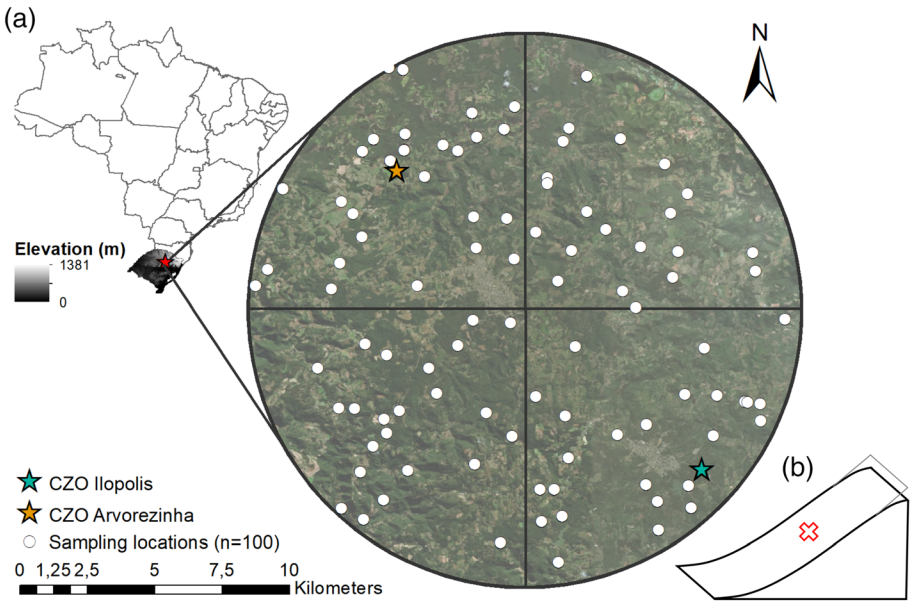

FIGURE 2. (a) Location of the study area at the edge of the Southern Brazilian Plateau in the state of Rio Grande do Sul (Brazil). Within the circular study area of 250 km^2, 100 sampling locations were selected. They are equally divided over the four quadrants and cover the widest possible range of slope gradients. The study area encompasses the critical zone observatories (CZO) of Arvorezinha (orange star) and Ilopolis (blue star). (b) All hillslopes were sampled in the middle of the linear sloping part (midslope position), indicated by the red cross.

ECDF) and the soil residence time, enabling us to get not only an estimate of long-term weathering rates but also of their evolution through time. By using this approach, the contribution of transported upslope soil material is explicitly taken into account, as this is inherent to our soil residence time calculations.

Synthetic model runs were performed for nine linear hillslopes with varying slope gradient, a slope length of 200 m and an initial uniform soil thickness of 20 cm. The choice of the initial soil thickness does not influence the final steady state thickness. The slope length and range of slope gradients was chosen based on the field sites (section 3.3.), with measured slope gradients ranging between 2.5° and 41° and mean a slope length of 200 m (range 60–500 m). We assume that incoming soil fluxes at the hillslope top are zero and use an open boundary condition at the lower end of our model domain. As such, topographic evolution is simulated as a function of influxes and outfluxes over the full domain, without imposing artificial boundary conditions. The depth of the interface between soil and parent material is determined by the soil production rate. Over time, the soil-mantled hillslope will develop profile convexities at the hillslope top (Figure 1, Gilbert, 1909; Kirkby, 1971). The model is set up with a horizontal resolution of 5 m and a time step of 1000 yr for a total period of 3 Myr: This time period is sufficient to reach steady state conditions (i.e., no change in soil thickness and *ECDF*) for all slopes tested.

3.3. Study Area and Sampling Strategy

The study area is located in the villages of Arvorezinha and Ilopolis in the state of Rio Grande do Sul (Brazil), on the southern edge of the Southern Brazilian Plateau (Vieira et al., 2015) (Figure 2a). This plateau is part of the Paraná-Etendeka magmatic province, with basalt and dacite-rhyolite as the main rock types (Caner et al., 2014; Turner et al., 1994). The basalt is often overlain by rhyolite (Renne et al., 1992). The dissected hilly landscape is characterized by a gentle to steep rolling topography (390 to 770 m above sea level) (Minella et al., 2014, 2008). Following the WRB classification (IUSS Working Group WRB, 2015), the main soil types are Acrisols, Cambisols, and Leptosols. The deep Acrisols are located on the flatter parts, whereas the shallower Leptosols and Cambisols are found on the steep slopes at the edge of the plateau (Minella et al., 2009). Bedrock mineralogy (two samples) determined by X-ray diffraction is dominated by sanidine (K-feldspar, ~45–55%) and fine grained quartz (~38%) (Vanacker et al., 2019). The bedrock elemental composition was characterized at 15 locations within the study area by Pelckmans (2018) and shows a domination of SiO_2

(67.16 ± 7.66%), followed by Al_2O_3 (13.64 ± 1.62%) and Fe_2O_3 (8.46 ± 4.07) with little regional variability. The climate is warm and humid subtropical with ocean influences and the absence of a dry season, corresponding to Köppen classification Cfb (Alvares et al., 2013; Peel et al., 2007). Mean annual precipitation on the plateau is ~1605 mm, well distributed throughout the year with average temperatures varying between 12 (July) and 22 °C (January) (Merten et al., 2010; Robinet, Minella, et al., 2018; Robinet, von Hebel., et al., 2018). The natural vegetation consists of mixed *Araucaria*-broadleaf forest in the north, changing to broadleaf subtropical forest in the south (Morellato & Haddad, 2000; Pillar & Quadros, 1999). Large-scale forest conversion to agricultural land started in the beginning of the twentieth century with the introduction of maize (*Zea mays*), soybean (*Glycine max*), erva-mate (*Ilex paraguariensis*), and tobacco (*Nicotina tabacum*) (Lopes, 2006).

Our study area matches a number of criteria that allow to successfully carry out a study on soil formation in soil-covered hilly landscapes: (i) It is underlain by a homogenous lithology so that variations in soil development between different locations are primarily related to topography, (ii) it has a relatively simple geologic-topographic history consisting of slopes formed by the incision of a near-horizontal plateau formed by igneous rocks over 100 Myr ago with minor tectonic deformation (Caner et al., 2014; Turner et al., 1994) so that slope development can be simulated using relatively simple assumptions on geologic history, (iii) it is located in an area with a subtropical climate which was not directly affected by glaciations, allowing for soil development over a long time period, and (iv) previously conducted research has produced a wealth of data on the study area (e.g., Robinet, Minella, et al., 2018; Robinet, von Hebel, et al., 2018; Schoonejans, 2016; Vanacker et al., 2019).

Within the 250-km^2 study area, 100 sampling locations were randomly selected using the KML random placemark generator of Google Earth. Sampling sites were distributed over the four quadrants, spanning the widest possible range of hillslope gradients. Sampling points were selected semirandomly: Randomly selected sampling points with similar slope gradient were manually moved to the nearest steeper or more gentle slope depending on the slope distribution within the quadrant (e.g., when the quadrant already contained many >10° slopes located close to each other, sites were selected on the nearest <10° slopes). The length of each slope—from the drainage divide down to the end of the linear sloping part—was determined in Google Earth. In this study, we do not account for land use type or history and sampled the widest possible range of slope gradients, encompassing cropland and forest.

Each selected hillslope ($n = 100$) was sampled at the midslope position. Slopes were measured in the field using a clinometer and locations were determined with a handheld GPS (Garmin Etrex Venture HC, horizontal accuracy: ±5 m). Soils were sampled with an Edelman auger (Eijkelkamp Soil & Water) down to the saprolite layer or to a maximum depth of 3 m. Identification of the different soil horizons was done according to the FAO guidelines (Jahn et al., 2006) where the saprolite layer was identified by using color (white to light yellow) and texture (loose, coarse-grained sandy material) as morphological indicators. Per horizon, one sample (~100 g) was collected from the center of the core to avoid contamination. If only the O-horizon was present, no sample was collected (locations F34, F35, F40, F47). Sampling sites have on average two to three horizons, with more horizons for deeper soils. All samples ($n = 222$) were air dried at a temperature of 40 °C, sieved at 2 mm, and the fine earth fraction was crushed using a mortar and pestle.

3.4. Application of the Be2D Model to Field Data

3.4.1. Determination of Weathering Indices From Soil Spectroscopy Data

Spectroscopy has proven to be a powerful tool in soil sciences, enabling to determine a variety of soil chemical properties based on their diagnostic absorption characteristics (Marco Nocita et al., 2015; Richter et al., 2009). In general, a higher predictive accuracy is obtained in the mid-infrared region (MIR) compared to the visible to near-infrared region (VIS-NIR) (Mohanty et al., 2016; Nocita et al., 2015; Soriano-Disla et al., 2014; Viscarra Rossel et al., 2006; Vohland et al., 2014). Here, we use data obtained by MIR-spectroscopy in order to quantify the weathering degree of the soil. The soil spectra are calibrated on 49 soil samples that cover the range of physico-chemical soil properties present in the area, and for which *CIA*, Fe_d/Fe_t, and *TRB* were determined from wet chemistry (Schoonejans et al., 2017; Vanacker et al., 2019, Text S1 and Table S1). Soil samples (49 for calibration and 222 other soil samples) were scanned in the MIR-region (FrontierTM with autosampler from PerkinElmer). By using partial least squares regression (PLS), the calibration function between the spectra and the three weathering indices was established. Best results were obtained

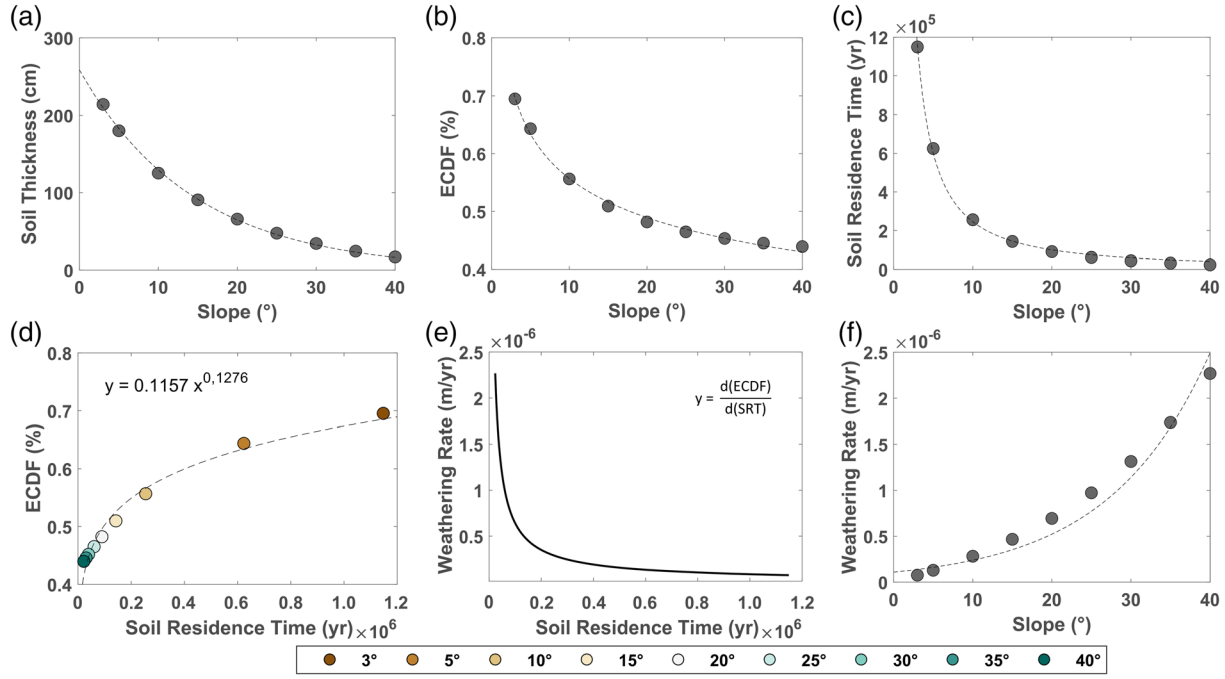

FIGURE 3. Modeled equilibrium soil thickness, weathering degree (given by the modeled extended chemical depletion factor (*ECDF*)) and modeled soil residence time (*SRT*) at the midslope position decrease with increasing slope gradient for the synthetic model runs (a–c). Higher than average values of soil residence time correspond with higher than average values of weathering degree (d) and lower than average values of derived weathering rates (e). The model runs show a positive relationship between the slope gradient and weathering rate (f). Dotted lines show the fitted relationships, which are exponential for slope gradient versus soil thickness (a) and weathering rate (f) and a power law for all other plots (b–d). The derivative of the fitted relationship between *ECDF* and *SRT* ($y = 0.1157\ x^{0.1276}$) is plotted in (e), which gives the model-derived weathering rate (change in *ECDF)* over time.

when using a snv-detrend (*dt*) preprocessing method with 6 PLS-factors for the *CIA* ($R^2 = 0.97$, RMSE = 1.67), *dt* with 3 PLS-factors for Fe_d/Fe_t ($R^2 = 0.84$, RMSE = 0.048), and multiplicative scatter correction (*msc*) with 7 factors for *TRB* ($R^2 = 0.91$, RMSE = 8.56). The best calibration function was then applied to the 222 soil samples to derive Fe_d/Fe_t, *CIA*, and *TRB* and assess uncertainties on these values. Uncertainties are obtained by following the method of Van de Broek and Govers (2019). For all sampling locations, a thickness-averaged weathering index is calculated. A detailed description of the calibration data set, calibration procedure, and uncertainty calculations is given in Text S3 and Figure S2.

3.4.2. Parameter Optimization

In order to better understand and explain the observed relationships from our field data and to obtain model-derived weathering rates and soil residence times for our sampling sites, the model is calibrated and applied to our sampling locations. For parameter optimization, each sampling location ($n = 100$) is simulated with its corresponding slope gradient and length. Hillslopes are assumed to be initially linear with a soil thickness of 20 cm and the model is set up with a horizontal resolution of 5 m, time step of 1000 yr and total model run time of 3 Myr. The parameter values for K, g_r, P_0, α, W_0, and β were optimized by evaluating the agreement between measured and modeled soil thickness at the midslope positions, as this is the location where soil thickness is determined in the field. The optimized parameter set is obtained using a genetic optimization algorithm (The MathWorks, 2020), as it has proven to be an efficient tool for finding global minima (Jelinski et al., 2019). Parameters are varied between realistic value bounds (Campforts et al., 2016; Jelinski et al., 2019), with $\alpha < \beta$ (respectively the soil production and chemical weathering depth scaling factors) as an additional constraint. This constraint was necessary as modeled *ECDF*-values otherwise increase with increasing soil thickness, which, according to our field results and the work of Burke et al. (2007), is not realistic. The Nash-Sutcliffe coefficient (*NS*) was used as objective function:

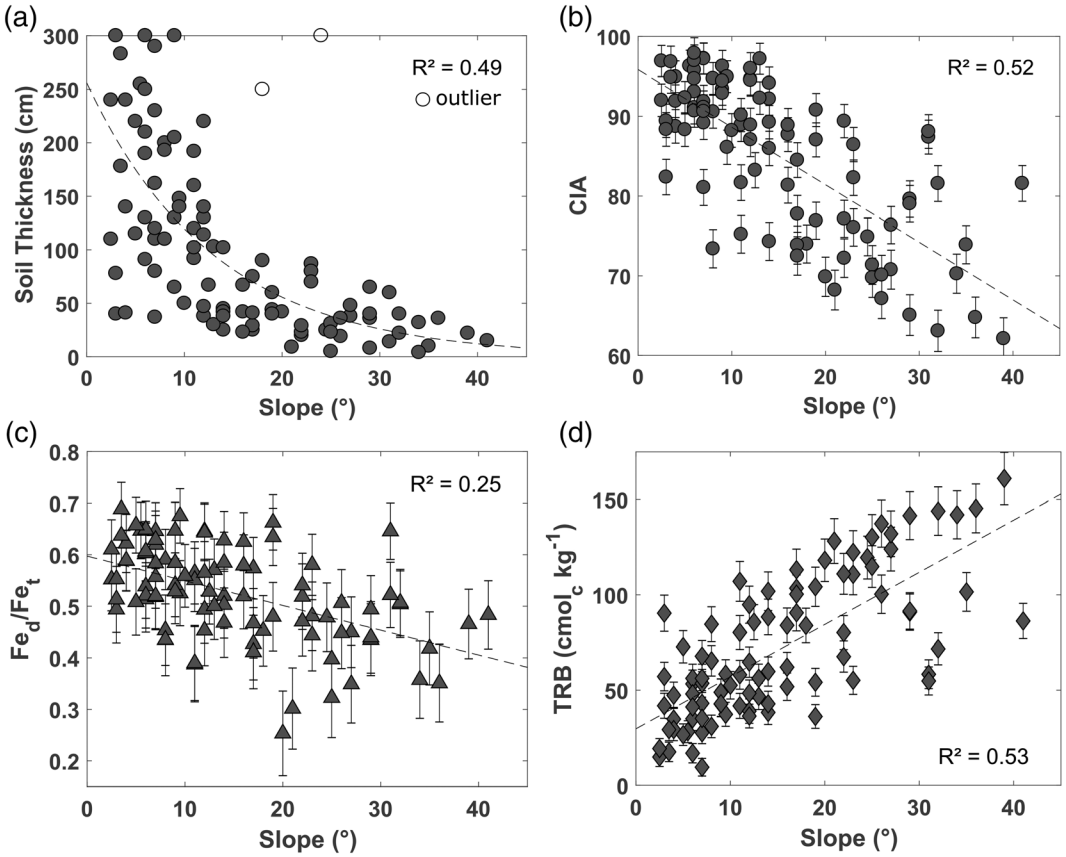

FIGURE 4. (a) Measured soil thicknesses at field sampling locations (n = 100) decline significantly with increasing slope gradient (n = 100) at the midslope position, following an exponential function (R^2 = 0.49, dashed line). Two locations show deviating results and are identified as outliers (standardized residuals >2.5). Weathering degrees, represented by the chemical index of alteration (*CIA*), iron ratio (Fe_d/Fe_t), and total reserve in bases (*TRB*), decrease significantly with increasing slope gradient at the midslope position in a linear way (dashed lines with R^2 of respectively 0.52, 0.25, and 0.53, b–d). Error bars show the standard deviation on the moving average of the residuals between mean modeled and measured values for 100 randomly chosen calibration (2/3) and validation (1/3) data sets (Text S3.3 and Figure S2).

$$NS = 1 - \left(\frac{\sum_{i=1}^{n} (O_i - M_i)^2}{\sum_{i=1}^{n} (O_i - \overline{O})^2} \right) \tag{21}$$

O_i is the measured soil thickness, M_i the modeled soil thickness, and $\overline{O}$ is the mean of the measured soil thicknesses at the 100 sampling locations. *NS* compares the magnitude of the residual variance to the measured data variance and ranges between $-\infty$ and 1, with 1 being the optimal value (Nash & Sutcliffe, 1970). A value of 1 indicates a perfect agreement between observations and simulations, whereas values smaller than 0 indicate that the model is not performing well, since the mean of the observed values is then a better predictor than the simulated value (Moriasi et al., 2007). Parameter dependency was evaluated by calculating the objective function when two parameter values are varied between their optimization bounds, keeping all other parameters at their optimal value.

4. Results

In this section the results of the synthetic model runs are first described, for which the optimized parameter values are used. Next, the observed relationships between slope gradient, soil thickness and weathering degree for the sampling sites are presented. Finally, the performance of the calibrated model is discussed, followed by the model-derived soil residence times and chemical weathering rates.

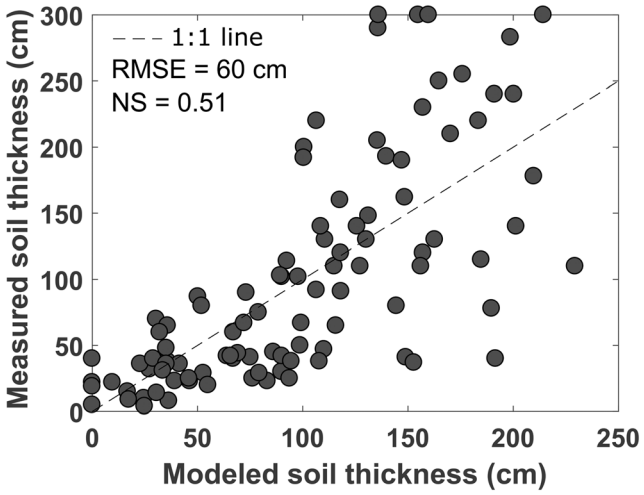

FIGURE 5. A Nash-Sutcliffe coefficient (*NS*) of 0.51 is obtained between modeled and measured soil thickness at the midslope position for the optimal parameter set. This corresponds to a RMSE of 60 cm.

4.1. Synthetic Model Runs

We first describe the results of the synthetic model runs using the optimized parameter values for the study site (see sections 3.4.2 and 4.3.1), where the weathering degree is represented by the simulated *ECDF*. Water erosion parameters m, n, and m_{ir} are assumed equal to, respectively, 1.1, 0.9, and 0.8 (Govers et al., 1994), with a value of 350 m for the transport capacity coefficient g_t (Govers et al., 1993; Van Oost et al., 2003). Soil bulk density was set at 1.35 g cm^{-3} based on values reported by Vanacker et al. (2019). The optimized parameter values for our field sites are used in the synthetic model runs: $K = 0.08$ cm yr^{-1}, $g_r = 1.32 \times 10^{-7}$ m yr^{-1} $P_0 = 7.92 \times 10^{-6}$ m yr^{-1}, $\alpha = 3.6 \times 10^{-3}$ cm^{-1}, $W_0 = 3.32 \times 10^{-6}$ m yr^{-1}, and $\beta = 7.92 \times 10^{-4}$ cm^{-1}. For *ECDF* weathering degrees Ti was used as the conservative element, as Zr can be lost from acidic soils (Schoonejans et al., 2017). We assumed that the concentration of Ti is homogenous in the parent material and equal to 5.7 g kg^{-1}, the average of earlier reported values for the area (Schoonejans, 2016; Vanacker et al., 2019). The model was applied to nine synthetic hillslopes of 200-m length with different slope gradients (3°, 5°, 10°, 15°, 20°, 25°, 30°, 35°, and 40°).

Figure 3a shows that the modeled steady state soil thickness decreases with increasing slope gradient, following an exponential relationship. The modeled *ECDF* (ranging between 0.44 and 0.69, Table S3) and soil residence time also decline with increasing slope gradient (Figures 3b and 3c) following a power function. This is to be expected, as lateral soil fluxes will increase with slope gradient, reducing soil thickness and soil residence time. As the *ECDF* represents the ratio of weathering over total denudation rate (equation 5), it also shows that weathering is dominant (*ECDF* > 0.5) for gentle slopes (<15°), moving toward an erosion dominated denudation regime for steeper slopes at the midslope position (Figure 3b). When the soil residence time is short, the timescale over which weathering processes can take place is also short, resulting in lower-than-average*ECDF* values and thus weathering degrees (Figure 3d). The change in weathering degree with soil residence time ($ECDF = 0.1157 \times SRT^{0.1276}$) is furthermore strongest for young soils developed on steep slopes, which are characterized by weathering rates up to 2.3×10^{-6} m yr^{-1} (Figures 3e and 3f). Weathering rates (derivative of *ECDF* over time) decrease strongly to 7.6×10^{-8} m yr^{-1} when soils become older (> ~200 kyr) and on more gentle slopes (<15°) (Figures 3d, 3e, and 3f). As the synthetic model is run with the optimized parameter values of the field sites (even though mineralogy is not accounted for), the maximum modeled *ECDF*-value of 0.69 seems realistic and indicates that the gentle slopes are maximally weathered, as the average bedrock composition of the study area consist of 38% quartz (Vanacker et al., 2019).

4.2. Field Measurements: Influence of Slope Gradient on Soil Thickness and Weathering Degree

At the 100 sampled midslope positions measured soil thicknesses vary between 4 and 300 cm, for slope gradients ranging between 2.5° and 41°. Soil thickness decreases significantly with increasing slope gradient following an exponential decline ($R^2 = 0.49$, Figure 4a). Two sampling locations (A1, A34) show deviating results for soil thickness. Having standardized residuals >2.5 (Figure 4a), they are considered as outliers and excluded from further analysis (more information can be found in Text S4). Variations in soil thickness for a given slope gradient indicate the heteroscedasticity of the data, with larger variations in soil thickness for gentle slopes compared to steep ones.

The weathering degree of the soil shows large variations with *CIA*-values ranging between 62 and 98, *TRB* values between 9 and 161 cmol$_c$ kg^{-1}, and Fe_d/Fe_t between 0.25 and 0.69 (Table S4). The weathering degree is negatively related to slope gradient (Figures 4b–4d). Highest R^2 values are obtained for a linear fit between the slope gradient and *CIA* ($R^2 = 0.52$), *TRB* ($R^2 = 0.53$), and Fe_d/Fe_t ($R^2 = 0.25$). However, a power relationship between slope gradient and weathering degree is equally likely, with R^2 values of 0.44, 0.53, and 0.23 for the *CIA*, *TRB*, and Fe_d/Fe_t, respectively (not shown in figure).

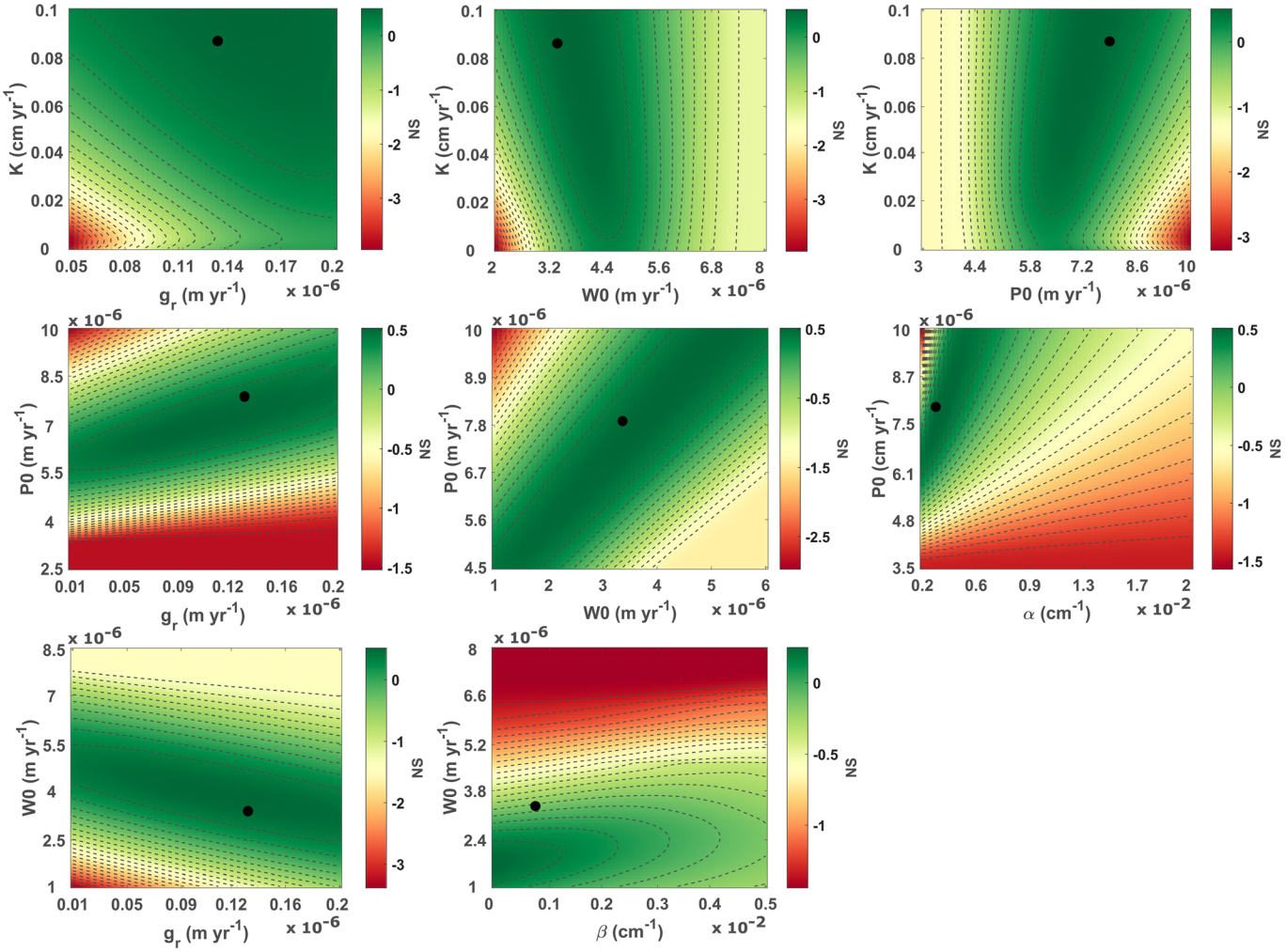

FIGURE 6. Objective functions used to constrain the parameter values, with the diffusive erosion transport coefficient (K), water erosion transport coefficient (g_r), soil production rate when soil thickness is zero (P_0), its depth-scaling factor (α), and the weathering rate when soil thickness is zero (W_0) and its depth-scaling factor (β), of the Be2D model, using the Nash-Sutcliffe coefficient (NS) as optimization criterion. In each plot the two parameter values range between realistic bounds, keeping all other parameters at their optimal value. Optimal parameter values, determined by the genetic optimization algorithm, are indicated by the black dots and might deviate from the lowest NS-value due to the imposed constraint ($\alpha < \beta$).

4.3. Model Application: Soil Residence Times and Weathering Rates

4.3.1. Model Performance

A single set of model parameters is optimized based on measured and modeled soil thickness for all observations (section 3.4.2). Optimal parameter values are $K = 0.08$ cm yr^{-1}, $g_r = 1.32 \times 10^{-7}$ m yr^{-1},$P_0 = 7.92 \times 10^{-7}$ m yr^{-1}, $\alpha = 3.6 \times 10^{-3}$ cm^{-1}, $W_0 = 3.32$ m yr^{-1}, and $\beta = 7.92 \times 10^{-4}$ cm^{-1}. For this parameter set we obtained a NS of 0.51, corresponding to a root-mean-square error (RSME) of 60 cm between modeled and measured soil thickness. Our model is thus capable of simulating the soil thickness-slope gradient relationship we observed. While agreement for individual observations is acceptable, observed soil thicknesses vary considerably for a given predicted soil thickness, especially for deeper soils (Figure 5). This is to be expected: Soil thickness is not simply a function of topography but will also vary depending on other factors such as local variations in hydrology and rheology of the parent material (Braun et al., 2016), which are not accounted for in our simulations.

Sensitivity runs are performed by calculating the objective function (NS) while allowing two parameters to vary within their optimization range, keeping all other parameters at their optimal value. This shows that no single parameter set can be considered as the unique optimal set (Figure 6). Optimal values of W_0, P_0, and α

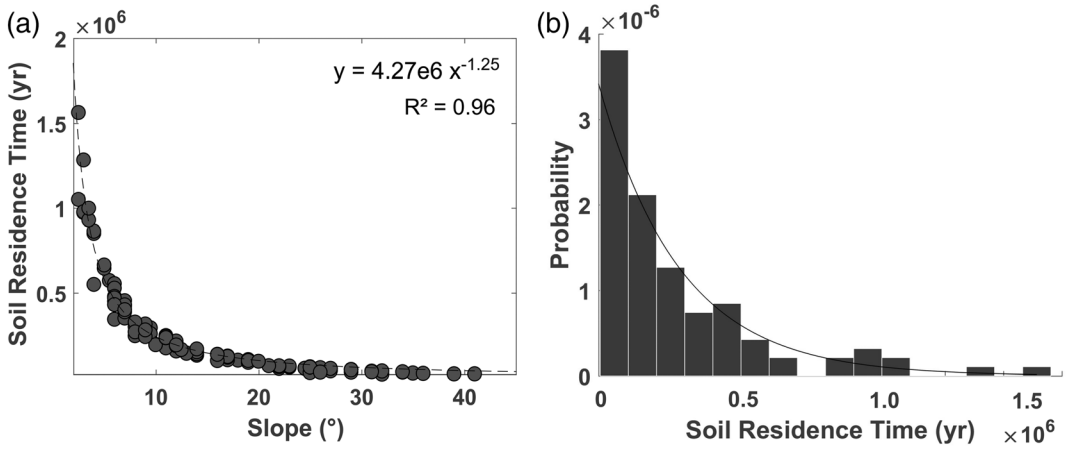

FIGURE 7. (a) Modeled soil residence times (*SRT*) for the sampled hillslopes at the midslope position approximately follow a negative power law relationship with slope gradient ($R^2 = 0.96$, dashed line). (b)*SRT*s at the midslope position are characterized by an exponential probability density function (black line).

are well constrained, whereas high *NS* values are obtained for a wide range of K and g_r values, which, respectively, determine the magnitude of diffusive soil transport and water erosion rates. A possible reason for this is that increasing erosion rates will be compensated by the optimized soil production (well-constrained P_0 and α), thereby allowing modeled soil thicknesses to be equal to measured soil thicknesses for a range of K and g_r values. Also, K and g_r values are negatively related: if a high diffusive erosion rate is assumed, optimal water erosion rates are low and vice versa. Only for W_0 versus β the optimal parameter value, as determined by the genetic optimization algorithm (black dot), does not fall in the area with the lowest *NS*. This is caused by the imposed constraint on the optimization algorithm ($\alpha < \beta$), resulting in higher optimized parameter values for β and W_0 than would be the case without this constraint. Optimal values of W_0 and P_0 are positively correlated, which is logical as an increase in soil production rates results in increasing weathering rates for a given value of physical erosion. The same is true for optimal values of P_0 and g_r, and P_0 and K: increasing the physical erosion rate will lead to higher soil production rates when all other parameters are kept constant (Figure 6).

4.3.2. Soil Residence Time

Modeled soil residence times for the sampled hillslopes at midslope position range between 22 and 1682 kyr, with a mean value of 290 kyr, and decrease as a power function with slope gradient ($R^2 = 0.96$, Figure 7a). The *SRT*s are characterized by an exponential probability density function (Figure 7b), therefore most

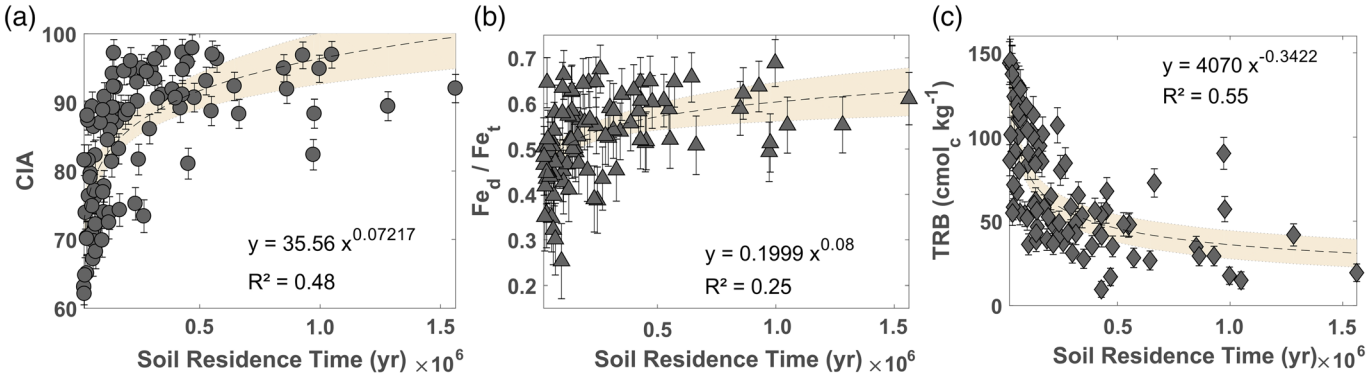

FIGURE 8. Measured soil weathering degrees, based on the chemical index of alteration (*CIA*), iron ratio (Fe_d/Fe_t), and total reserve in bases (*TRB*), increase strongly with simulated soil residence times (*SRT*). For *SRT*s below ~200 kyr there is a rapid increase of chemical weathering degree with *SRT*. Shaded areas around the dashed trend line indicate the 95% functional confidence interval bounds of the fitted power function. Error bars show the standard deviation on the moving average of the residuals between mean modeled and measured values for 100 randomly chosen calibration (2/3) and validation (1/3) data sets (Text S3.3, Figure S2).

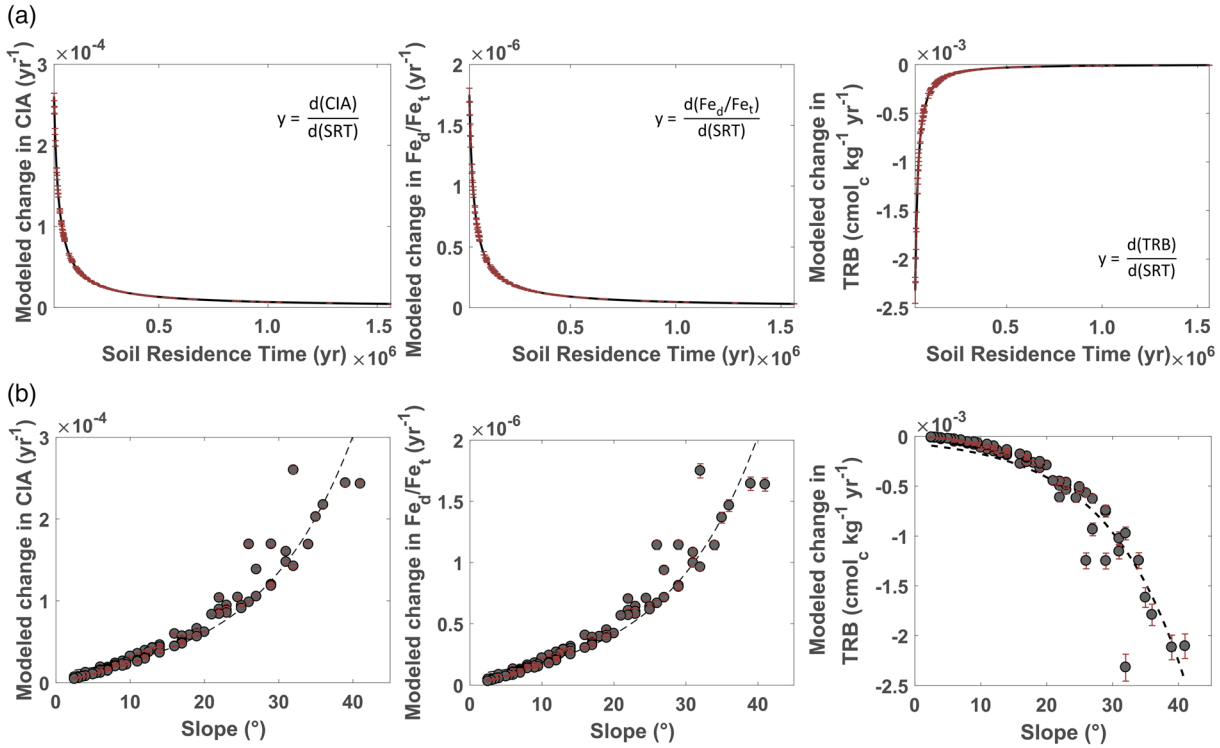

FIGURE 9. (a) Modeled changes in chemical index of alteration (*CIA*), iron ratio (Fe_d/Fe_t), and total reserve in bases (*TRB*) (calculated as the derivative of the relationship between *CIA*, Fe_d/Fe_t, and *TRB* and soil residence time (SRT), Figure 8), at the midslope position decrease strongly with increasing *SRT* and stabilizes after 218, 220, and 143, respectively. (b) Modeled changes in weathering indices at the midslope position increase with slope gradient (exponential fit indicated by dashed line). Error bars indicate the 95% functional confidence interval bounds on the fitted power function between the weathering index and *SRT* (Figure 8).

hillslopes have a *SRT* below this average value. Very high *SRT* values are obtained for a limited number of observation points (corresponding to gentle slopes). As can be expected, modeled *SRT*s are positively correlated with soil thickness (not shown).

A relationship between the measured weathering indices (*CIA*, Fe_d/Fe_t, and *TRB*), which reflect the weathering degree, and the simulated soil residence time can now be established (Figure 8). Logically, soils with a short residence time are characterized by a low weathering degree, which increases strongly when soils become older and more intensely weathered. The observed power relationships indicate that soil chemical weathering degree is highly sensitive to soil residence time for *SRT*s less than ~200 kyr. Once *SRT*s are higher than 200 kyr, the chemical weathering indices show maximum depletion and become almost insensitive of time. This points to a supply-limited weathering system, where the chemical weathering is limited by the supply of fresh material.

4.3.3. Chemical Weathering Rates

An estimate of the long-term weathering rates can now be obtained for the field data by taking the derivative of the relationship between the weathering degree (given by the measured *CIA*, Fe_d/Fe_t, and *TRB*) and soil residence time (shown in Figure 8). This derivative is taken over a 1-yr time interval at the last modeling time step where all hillslopes are in steady state. This gives the change in weathering degree over time, or the weathering rate (Figure 9). As weathering indices are relative measures of weathering degree, the derived weathering rates should also be interpreted as the rate at which weathering indices change relative to their reference value, not as absolute rates. The modeled changes in weathering indices are a power function of soil residence time (Figure 9a), similar to what was observed for the evolution of *ECDF* in the synthetic model runs (Figure 3): older soils are weathered at a rate far slower than younger soils that contain more fresh material. It is clear that weathering rates stabilize at a given *SRT*, after which they become low and time-invariant. This stabilization time is quantified as the time where the change in weathering rate is

less than 1% of the total change. Chemical weathering rates stabilize after 218 kyr when considering the *CIA*, 220 kyr for Fe_d/Fe_t, and 143 kyr for *TRB*.

This indicates that chemical stabilization requires a time span of hundreds of thousands of years, thus far longer than the length of the Holocene, and that it depends on the weathering index used.

Modeled weathering rates (derived as changes in weathering degree) increase with increasing slope (Figure 9b), as was the case for the synthetic runs (Figure 3). The increase of weathering rate with slope gradient in the synthetic runs can be ascribed to the presence of more fresh soil material on steeper slopes due to higher erosion rates, leading to higher soil production rates. While this is likely to be the most important mechanism at our field sites, other processes such as the increase of lateral soil water fluxes with distance from the divide may reinforce this trend. Modeled changes in weathering degree vary up to 2 orders of magnitude depending on slope gradient. An overview table with details on total soil thickness, slope, weathering degrees (*CIA*, Fe_d/Fe_t, and *TRB*), modeled soil residence time and weathering rates for all sampled hillslopes can be found in Table S4.

5. Discussion

5.1. Controls on Soil Thickness

At our field site, an exponential fit between slope gradient and measured soil thickness at midslope explains ~49% of the observed variability for slopes between 2.5° and 41° (Figure 4a). Several earlier studies observed a strong relationship between soil thickness and slope gradient. However, the exponential decline of soil thickness with slope we found is different from the earlier reported power relationship for a site in New-Zealand (Derose et al., 1993) and the linear relationship found in south-eastern Spain (Reaney, 2003). Important to note is that in these studies samples were taken at different hillslope positions, which can lead to significantly different soil thicknesses for equal slope gradient and curvature (Catani et al., 2010). The variability in soil thickness data makes it difficult to identify the precise nature of the slope gradient-soil thickness relationship: when applying a power and linear relationship to our data, R^2 values decrease to, respectively, 0.39 and 0.43. However, our model results also suggest that an exponential relationship is more likely than a linear or power one (Figure 3a). A key factor explaining the exponential decrease of soil thickness with slope gradient in the model study is that we assume that soil production decreases exponentially with soil thickness, as has been documented by several studies (Dixon et al., 2009; Heimsath et al., 1997, 1999; Small et al., 1999). This can be illustrated with the following thought experiment.

Let us assume that soil production is constant and depth-independent and that only diffusive erosion is present, while water erosion and weathering are assumed to be zero. At steady state the diffusive flux at the steepest slope now has to be in equilibrium with the total (constant) soil production upslope of the steepest slope location. As the diffusive flux is assumed to be proportional to the product of soil thickness and slope, doubling the slope gradient at the midslope location will now result in halving the soil thickness at that location, resulting in a reciprocal relationship between soil thickness and slope gradient. However, when soil production is assumed to decrease with soil thickness, soil thickness at the midslope location will be higher than predicted by this relationship when the slope is steep. This is because soil production rates will be higher on steep slopes where soils are thin. If water erosion is present this will strengthen the effect of slope gradient on soil thickness, because water erosion will remove more soil from steeper slopes, thus counteracting the effect of increasing soil production with increasing slope gradient. We assume soil weathering to be negatively exponentially related to soil thickness: Soil weathering will therefore covary with soil production rates leading to increased soil removal by weathering at locations where soil production is high. Again, this will reduce the soil thickness more strongly at locations where soils are already thin, that is, steep slopes.

In our modeling framework, we apply the same assumptions as outlined in the above thought experiment. Therefore, we simulate a concave upward relation between slope gradient and soil thickness that is described by an exponential function rather than a reciprocal function, as soil thickness does not decrease as rapidly with slope gradient as predicted by the latter. This relationship can be described by an exponential function and is validated by our field data. Next to the discussed interaction between different erosion processes and soil formation, all depending on slope gradient, multiple studies have shown that also slope curvature significantly influences soil thickness variations (e.g., Catani et al., 2010; Minasny &

McBratney, 2001; Thompson et al., 2006). We argue that curvature is not strongly altering our results since our sampling sites are located at the middle of the linear hillslope section, where profile curvature is zero. Furthermore, our sampling sites have minimal plan curvature so that we can safely assume that curvature does not significantly affect measured soil thicknesses. If the impact of curvature were to be assessed this would require multiple sampling location along the hillslope transect and extending the current 2-D model to three dimensions (Campforts et al., 2017).

Large variations in soil thickness are present on slopes up to 15°, where for the same slope gradient soil thickness can range between 50 and 300 cm (Figure 4a). This large scatter in soil thickness is absent on steeper slopes. We attribute this difference to the fact that the dominant control on soil thickness is different on gentle versus steep slopes. Soil thickness on steep slopes is mainly controlled by lateral soil movement: The main control on soil thickness is that the lateral soil flux has to be in equilibrium with soil production (minus weathering) over the entire upslope section. Out-of-equilibrium soil thicknesses cannot persist: if soil thicknesses were too small, they would increase rapidly until equilibrium reestablished, while soils that are too thick would be rapidly removed by erosion. On the lower slope gradients, lateral soil fluxes will be much lower and soil thickness becomes much more dependent on the magnitude of local soil production and local weathering rates. Hereby local variations can be reinforced by local feedbacks, for example, because variations in regolith thickness lead to the concentration of water (and hence weathering) in those areas where regolith thickness is highest. Consequently, larger variations in soil thickness can be maintained on gentle slopes. The dominance of vertical fluxes on lower slope gradients is also evidenced by the high degree of weathering on low-gradient slopes (Figures 4b–4d). This is confirmed by changes in modeled *ECDF*-values (Figure 3): On gentle slopes (<15°) chemical weathering dominates ($ECDF > 0.5$), with an increasing dominance of physical erosion rates ($ECDF < 0.5$) for steeper slopes at the midslope position, similar to the results of Burke et al. (2007). Recent reactive transport modeling has shown that regolith thickness can indeed be predicted by simulating chemical weathering and water and solute fluxes (Egli et al., 2018; Maher & Navarre-Sitchler, 2019). Increasing vertical flowrates leads to higher regolith thickness because chemical weathering rates and soil production rates are both proportional to flow rates (Egli et al., 2018; Hunt & Ghanbarian, 2016; Lebedeva & Brantley, 2013; Maher, 2010; Maher & Navarre-Sitchler, 2019). Thus, although the current version of Be2D does not allow to do this, it would in principle be possible to simulate local variations in soil production and weathering by explicitly accounting for local variations in hydrological and lithological conditions. However, running such a model to successfully predict local variations in soil thickness would require detailed data on local bedrock properties and hydrological conditions along entire hillslopes, which are not available.

5.2. Model Verification: Comparison With Independent Field Measurements

After optimizing the model by comparing modeled with measured soil thickness at the midslope position for all sampled hillslopes (slope gradients between 2.5° and 41°), total denudation rates range between 3.5×10^{-6} m yr^{-1} and 7.9×10^{-6} m yr^{-1} and total erosion rates vary from 6.8×10^{-7} m yr^{-1} to 10.9×10^{-6} m yr^{-1}. We determined weathering rates by taking the derivative of the weathering degree over soil residence time. For the synthetic model runs these rates are obtained by looking at the change in modeled *ECDF* over time at the final time step when soils are in steady state. This results in weathering rates between 7.6×10^{-8} m yr^{-1} and 2.3×10^{-6} m yr^{-1}, depending on slope gradient. These modeling outcomes are in very good agreement with independently obtained field measurements of the CZO in our study area based on in situ ^{10}Be and *CDF* measurements (using Ti as conservative element) by Schoonejans et al. (2017). They obtained total denudation rates at the hillslope convexity that vary between 2.0×10^{-7} m yr^{-1} and 5.2×10^{-6} m yr^{-1}, chemical weathering rates varying from 7×10^{-8} m yr^{-1} to 1.9×10^{-6} m yr^{-1}, and erosion rates between 1.0×10^{-7} m yr^{-1} and 3.3×10^{-6} m yr^{-1}. Schoonejans et al. (2017) furthermore constrained minimum soil residence times at the hillslope convexity based on meteoric ^{10}Be between 146 and 185 kyr, after correcting for ^{10}Be losses due to leaching. Again, these minimum ages correspond well with the average residence time of 290 kyr that we obtained. This indicates that our model is able to simulate realistic soil residence times based on the modeled erosional fluxes.

A potential limitation on our *ECDF* calculations is that we assume that the saprolite chemistry is constant along the hillslope and throughout time. As saprolite weathering degree and rate also vary with erosion rates (Dixon et al., 2009, 2012) this simplification might affect the modeled *ECDF* values. This may, on its turn,

have an impact on the relationship between modeled soil residence times and *ECDF* and thus on the derived weathering rates we obtained. Weathering indices, which are based on relative changes in elemental composition, are not suitable for the derivation of absolute weathering rates. This is because they do not explicitly take into account the composition of the bedrock and are not based on a conservative element. Rather, they indicate the transformation of soil minerals instead of the total amount of soil lost due to chemical weathering. These weathering indices, however, proved a useful tool in examining the relationship between topography and soil chemical weathering as they can be interpreted in a relative fashion, independently confirming the obtained relationships between topography and soil chemical weathering degree and rate from the synthetic model runs (Figures 3, 4, 8, and 9). Furthermore, they enabled us to obtain an estimate of the timescale at which chemical weathering degrees and rates become time-invariant, which is around 200 kyr for *CIA* and Fe_d/Fe_t and 150 kyr for *TRB* (Figures 8 and 9). This implies that soil development requires more or less stable climatic conditions for more than hundred thousand years to arrive at steady state.

5.3. Topographic Imprint on Weathering Degrees Is Dictated by Soil Residence Times

Both our synthetic modeling results and field observations show a negative relationship between weathering degrees and slope gradient (Figures 3 and 4). Gentle hillslopes are characterized by high weathering degrees, which decrease when slopes become steeper. The clear relationship we observed in the field is likely due to the fact that spatial variations in confounding factors such as precipitation, temperature, and lithology are limited in our study area. Dixon et al. (2012) found that the theoretically predicted decrease of *CDF* with slope gradient was not consistently observed in the field and attributed this to the obliterating effect of local variations in variables controlling soil production and weathering.

In semiarid regions both a positive (Osat et al., 2016) and a negative (Burke et al., 2007) relationship between weathering degree and slope gradient was observed. In the study of Osat et al. (2016) this relationship seems to controlled by site-specific conditions where soil development appears to be driven more by water availability than transport processes, as wetter areas were found on steeper slopes allowing the accumulation of mobile cations. Burke et al. (2007) also explain the differences in weathering degrees as the consequence of water availability: They argue that increasing overland flow on steep slopes reduces infiltration and thereby the amount of water that may drive weathering. While water availability might indeed be an important explanatory factor in these semiarid environments, we do not think that this is the main explanatory factor in our study area where precipitation is abundant. It is more likely that the main cause of the observed variation in chemical weathering degree with slope gradient is that soil residence times are much lower on steeper slopes (Figure 7) and that therefore the time available for weathering is much smaller, resulting in lower weathering degrees (Figures 3d and 8). Thus, the inverse slope-weathering degree relationship is not due to the local conditions on the steep slope: rather, it is a consequence of how the entire soilscape is formed. Our findings confirm that geomorphic processes can lead to soil rejuvenation as described by Chadwick and Asner (2016). They showed that in the tropical Peruvian Amazon, soil nutrient distribution depends on hillslope gradient and topographic position: Flat stable locations are most depleted in available nutrients compared to steeper convex regions. Similarly, in a semiarid environment in Colorado, Wyshnytzky et al. (2015) found clear soil development on gentle slopes and poor soil development on moderate to steep slopes.

5.4. Positive Relationship Between Weathering Rate and Slope Gradient Suggests Supply-Limited Conditions

The positive relationship between the increasing change in both model-derived *ECDF* (Figure 3f) and measured *CIA*, Fe_d/Fe_t, and *TRB* (Figure 9b) with slope gradient indicates that on steeper slopes weathering processes are faster than on gentle ones. This is not a causal relationship: we argue that the relation between weathering rates and slope gradient is a consequence of the relationship between slope gradient and soil residence time, where younger soils on steep slopes contain more fresh material due to increased soil rejuvenation, thereby enabling faster chemical reactions. This might on its turn also explain the negative relationship that is observed between chemical weathering rates and soil thickness for our data (not shown) and by Burke et al. (2007, 2009). Deeper soils typically have long soil residence times, leading to a depletion in weatherable minerals and lower weathering rates. This coupling between soil residence time and soil thickness might,

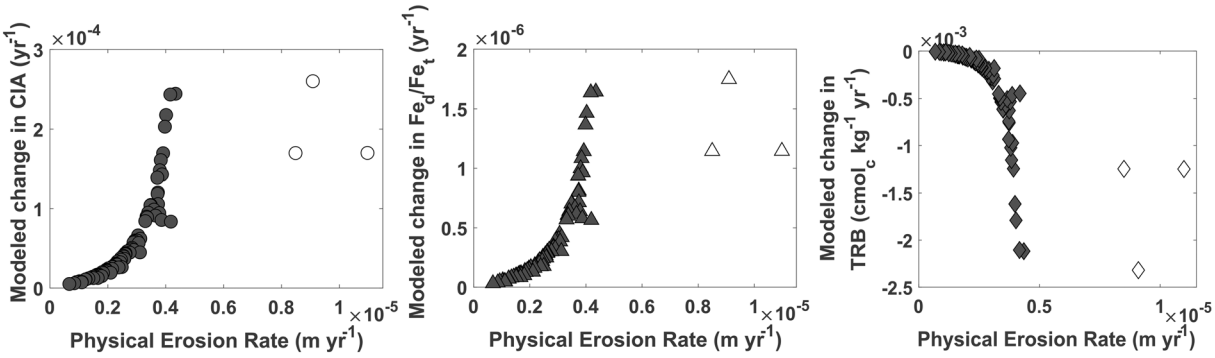

FIGURE 10. Modeled changes in (left) chemical index of alteration (*CIA*), (middle) iron ratio (Fe_d/Fe_t), and (right) total reserve in bases (*TRB*), obtained as the derivative of these indices over time and interpreted as weathering rates, are positively related to modeled physical erosion rates. This suggests the dominance of supply-limited weathering conditions. Points that strongly deviate from this relationship (A23, A35, and F43) are indicated by hollow symbols. These locations are marked by very long and/or steep hillslopes, resulting in a modeled soil thickness equal to zero at the midslope position.

however, be more apparent in sloping, and therefore eroding, landscapes like ours and the study sites of Burke et al. (2007, 2009).

Chemical erosion rates have typically been divided into two end-member regimes: supply-limited and kinetically limited chemical erosion (Dixon et al., 2009, 2012; Ferrier et al., 2016; Gabet, 2007; Lebedeva et al., 2010; Lebedeva & Brantley, 2013; Riebe et al., 2017). In the first case chemical erosion rates increase proportionally with rates of fresh supply from regolith production, as weathering reactions are fast enough to chemically erode all the supplied reactive materials away (Hilley et al., 2010; Lebedeva et al., 2010). Under the kinetic-limitation the chemical weathering rate solely depends on kinetic factors as temperature and fluid chemistry, being insensitive to differences in supply rates as there is plenty of weatherable material available (Riebe et al., 2017; Schoonejans et al., 2016). As erosion rates are considered as a proxy for mineral supply rates, the presence or absence of a relationship between erosion and chemical weathering rates can be used to distinguish between these two end-member regimes (Ferrier et al., 2016; Riebe et al., 2017).

Our modeled weathering rates increase with increasing slope gradient (Figures 9b and 3f), which suggests that weathering rates are also positively related to modeled physical erosion rates. This is confirmed by our modeling outcomes (Figure 10). Hence, this positive coupling between weathering rates (derived as the change in *CIA*, Fe_d/Fe_t, and *TRB* over time) and physical erosion rates suggests that our study area can be classified as a supply-limited environment. This is in agreement with the theoretical modeling outcomes of Gabet and Mudd (2009) and Dixon et al. (2012): The positive relationship between weathering and erosion is one of diminishing returns and might even become negative when an erosion threshold value (above 100 ton km^{-2} yr^{-1}) is exceeded and the system becomes kinetically limited. As our study area is characterized by very low erosion rates (0.9–14 ton km^{-2} yr^{-1} based on our modeling results), we are far below this limit and therefore in supply-limited conditions. This might have several implications: (i) a stronger dependence of weathering rates on fluid flow, pH, and mineral solubility than on mineral surface area and mineral kinetics, (ii) a dampened temperature dependence, and (iii) erosion accelerated weathering (Maher, 2010). This does not imply that weathering on these slopes has always been supply-limited. A transient erosion pulse that travels through this landscape might (temporarily) induce kinetically limited conditions. The occurrence of such an erosion pulse is realistic given that our study area is located at the edge of a plateau. Understanding in detail how such a pulse may affect landscape development requires new, three-dimensional models, wherein the physiochemical soil continuum can be coupled to fluvial dynamics, regulating large-scale transient landscape response through the propagation of incision waves (Bishop et al., 2005; Campforts et al., 2017; Campforts & Govers, 2015; Shobe et al., 2017).

5.5. Soil Residence Times: Differences With Soil Age, Scale Dependency, and Relation With Weathering Rates

In stable, noneroding landscapes (e.g., glacial moraines and fluvial terraces), weathering rates can be obtained by dividing the mass loss during soil formation by the age of the geomorphic surface (soil age)

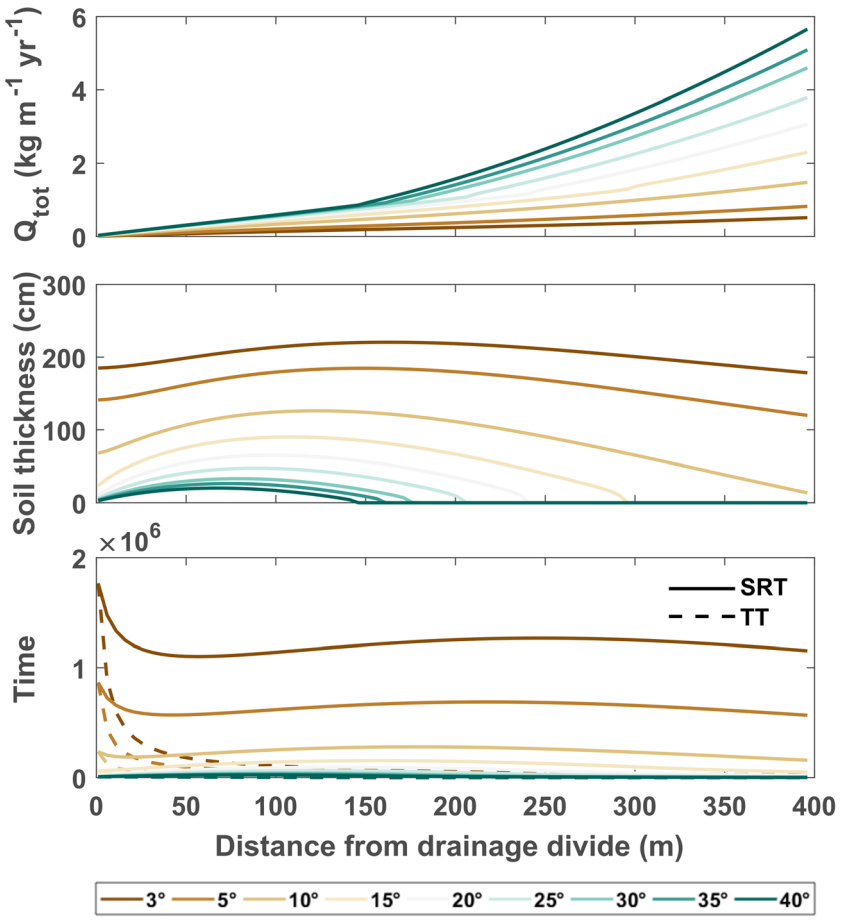

FIGURE 11. (top) Modeled total erosional fluxes (Q_{tot} [kg m^{-1} yr^{-1}]) increase strongly with increasing distance from the drainage divide and are highest for steep slopes. (middle) Soil thickness generally decreases with increasing distance from the drainage divide as erosion fluxes increase, which might even lead to the total absence of soil for the steepest slopes. (bottom) Modeled turnover time (*TT*) strongly decreases with increasing distance from the divide in the first tens of meters from the drainage divide, as total soil fluxes strongly increase with distance downslope. Modeled soil residence times (*SRT*), on the other hand, stay relatively stable along the hillslope, as the relative proportion of young particles increases downslope. These results are for synthetic model runs with a slope length of 400 m instead of 200 m in order to clearly show variations along the hillslope, keeping all other parameters identical to the other synthetic model runs (sections 3.2 and 4.1).

(Bain et al., 1993; Chadwick et al., 1990; Merritts et al., 1991; White & Brantley, 2003). In sloping terrains the age of the landform, however, is irrelevant, as the soil experiences constant rejuvenation due to local soil production and removal by sediment transport, necessitating the use of soil residence times instead of soil ages to determine weathering rates (Mudd et al., 2014; Yoo et al., 2007, 2009). By applying reservoir theory on both eroding and noneroding landscapes with different mixing regimes, Mudd and Yoo (2010) showed that soil production, transport, mixing, and dissolution processes should be taken into account when determining soil residence times and that the soil residence time can be twice as high as the soil age. Estimated weathering rates may therefore differ strongly based on how the time period over which weathering took place is estimated, where it can then be expected that weathering rates are higher when using soil age instead of soil residence time (Mudd & Yoo, 2010).

Soil residence times are calculated as the flux-weighted average of the particle transit times (which decrease with increasing distance from the drainage divide, see Text S2 and Figure S1). The soil at a given hillslope position will therefore consist of particles of different ages with very young particles resulting from local soil production and some very old particles that originated near the hilltop. The age mix of these particles may be expected to change along the slope. This raises the question to what extent soil residence time may depend

on the exact location on the hillslope that is being sampled and on the hillslope scale. Synthetic model runs (for hillslopes with varying slope gradient and a slope length of 400 m using our optimized parameter set) show that modeled soil residence times are rather constant along the hillslope transect (Figure 11). Only at the first tens of meters from the drainage divide *SRT*s are higher compared to the rest of the slope. This is the area where a convexity is formed, resulting in lower slope gradients and relatively deep soils in combination with low erosional fluxes and high turnover times (TT). Soil residence times are relatively independent of slope length and thus scale, but are highly determined by slope gradient (Figure 11). The observation that soil fluxes do increase with slope length, while soil thickness decreases when a certain downslope distance is exceeded, is explained by the importance of water erosion: Water erosion becomes more important with increasing slope length, thereby allowing the total soil flux to increase strongly with slope length, resulting in decreasing soil thickness. This also implies that our finding that soil residence times are relatively constant once a hillslope length of ~50 m is exceeded is not general: the pattern may be significantly different depending on the rate of soil production and on the relative importance of water erosion to diffusive erosion.

6. Conclusions

Variations in soil thickness and weathering degree in our subtropical study area in Southern Brazil are strongly linked to topography, as both decline with increasing slope gradient. By using interrelationships between slope gradient, soil thickness, and weathering degree, we could calibrate an enhanced version of the Be2D model, simulating long-term hillslope fluxes in combination with soil formation and weathering. Combining a numerical soil-landscape evolution model with field data allowed us to gain insight and make inferences about the relationships between soil thickness and topography with weathering degrees and rates. Modeled chemical weathering rates based on *ECDF* show that, also when weathering is in steady state, chemical weathering rates might vary 2 orders of magnitude depending on slope gradient. Weathering rates are positively related to modeled erosion rates. This confirms earlier studies in soil-mantled landscapes: Erosion rates are not high enough and soil thickness not small enough to observe a decline in weathering rates with increasing erosion, which may be found in actively uplifting mountain areas. Combining the numerical model with field data enabled us to obtain model-derived soil residence times and chemical weathering rates. As such we can now propose a long-term spatiotemporal framework for soil development in this subtropical region. Soil residence times are calculated by taking into account both local soil production and material transported from upslope positions and vary between ~20 and 1700 kyr, with an average value of ~290 kyr. This shows that in a soil-mantled area a long time is required to develop a steady state soilscape. This is not only because soil formation processes are inherently slow but also because it takes a long time to reach an equilibrium between topography and soil properties, where it takes ~150 to 200 kyr to obtain fully weathered soils with stabilized chemical weathering rates. We found that the development of an equilibrium soilscape in our study area, with climatic and lithological conditions favorable to soil development, takes several hundreds of thousands of years. As soil mantles in many areas are much younger than this, these soilscapes will often be out of equilibrium. The integrated modeling approach we present here may be especially useful to further our understanding of soilscapes in such transient conditions.

Acknowledgments

This research has been supported by the Belgian Development Cooperation through VLIR-UOS. VLIR-UOS supports partnerships between universities and university colleges in Flanders (Belgium) and the South looking for innovative responses to global and local challenges. This study was supported by the Belgian Science Policy Office (BelSPO) in the framework of the Inter University Attraction Pole project (P7/24): SOGLO—The soil system under global change. L. Brosens and B. Campforts received, respectively, a doctoral (11B6919N) and postdoctoral (12Z6518N) grant from the Research Foundation Flanders (FWO). We would like to thank the team of the Department of Soils of the University of Santa Maria (RS, Brazil) for their help during the field campaign. Data sets for this research are available at Brosens et al. (2020). We would like to thank Pedro Val and two other anonymous reviewers for their constructive and extensive feedback, enabling significant improvement of the manuscript.

References

Almond, P., Roering, J., & Hales, T. C. (2007). Using soil residence time to delineate spatial and temporal patterns of transient landscape response. *Journal of Geophysical Research*, *112*, F03S17. https://doi.org/10.1029/2006JF000568

Alvares, C. A., Stape, J. L., Sentelhas, P. C., de Moraes Gonçalves, J. L., & Sparovek, G. (2013). Köppen's climate classification map for Brazil. *Meteorologische Zeitschrift*, *22*(6), 711–728. https://doi.org/10.1127/0941-2948/2013/0507

Ameijeiras-Mariño, Y., Opfergelt, S., Schoonejans, J., Vanacker, V., Sonnet, P., de Jong, J., & Delmelle, P. (2017). Impact of low denudation rates on soil chemical weathering intensity: A multiproxy approach. *Chemical Geology*, *456*, 72–84. https://doi.org/10.1016/j.chemgeo.2017.03.007

Anderson, R. S. (2015). Particle trajectories on hillslopes: Implications for particle age and ^{10}Be structure. *Journal of Geophysical Research: Earth Surface*, *120*, 1626–1644. https://doi.org/10.1002/2015JF003479

Anderson, S. P., Dietrich, W. E., & Brimhall, G. H. (2002). Weathering profiles, mass-balance analysis, and rates of solute loss: Linkages between weathering and erosion in a small, steep catchment. *Bulletin of the Geological Society of America*, *114*(9), 1143–1158. https://doi.org/10.1130/0016-76010.1130/0016-7606(2002)114<1143:WPMBAA>2.0.CO

Bain, D. C., Mellor, A., Robertson-Rintoul, M. S. E., & Buckland, S. T. (1993). Variations in weathering processes and rates with time in a chronosequence of soils from Glen Feshie, Scotland. *Geoderma*, *57*(3), 275–293. https://doi.org/10.1016/0016-7061(93)90010-I

Bishop, P., Hoey, T. B., Jansen, J. D., & Lexartza Artza, I. (2005). Knickpoint recession rate and catchment area: The case of uplifted rivers in eastern Scotland. *Earth Surface Processes and Landforms*, *30*(6), 767–778. https://doi.org/10.1002/esp.1191

Bland, W. J., & Rolls, D. (2016). Weathering: An introduction to the scientific principles). *Weathering: An introduction to the scientific principles*. Abingdon: Routledge. https://doi.org/10.4324/9781315824918

Brantley, S. L. (2008). Understanding soil time. *Science*, *321*(5895), 1454–1455. https://doi.org/10.1126/science.1161132

Braun, J., Mercier, J., Guillocheau, F., & Robin, C. (2016). A simple model for regolith formation by chemical weathering. *Journal of Geophysical Research: Earth Surface*, *121*, 2140–2171. https://doi.org/10.1002/2016JF003914

Brimhall, G. H., & Dietrich, W. E. (1987). Constitutive mass balance relations between chemical composition, volume, density, porosity, and strain in metasomatic hydrochemical systems: Results on weathering and pedogenesis. *Geochimica et Cosmochimica Acta*, *51*(3), 567–587. https://doi.org/10.1016/0016-7037(87)90070-6

Brosens, L., Campforts, B., Robine, J., Vanacker, V., Opfergelt, S., Ameijeiras-Mariño, Y., et al. (2020). Data for: Combination of numerical modelling and field measurements reveals strong regional control of slope on soil thickness and chemical weathering in subtropical Brazil. https://doi.org/10.17632/fxmn7p6fb4.1

Buol, S. W., Southard, R. J., Graham, R. C., & McDaniel, P. A. (2011). *Soil genesis and classification*. Oxford, UK: Wiley-Blackwell. https://doi.org/10.1002/9780470960622

Burke, B. C., Heimsath, A. M., Dixon, J. L., Chappell, J., & Yoo, K. (2009). Weathering the escarpment: Chemical and physical rates and processes, south-eastern Australia. *Earth Surface Processes and Landforms*, *34*, 155–161. https://doi.org/10.1002/esp.1764

Burke, B. C., Heimsath, A. M., & White, A. F. (2007). Coupling chemical weathering with soil production across soil-mantled landscapes. *Earth Surface Processes and Landforms*, *32*, 853–873. https://doi.org/10.1002/esp.1443

Campforts, B., & Govers, G. (2015). Keeping the edge: A numerical method that avoids knickpoint smearing when solving the stream power law. *Journal of Geophysical Research: Earth Surface*, *120*, 1189–1205.

Campforts, B., Schwanghart, W., & Govers, G. (2017). Accurate simulation of transient landscape evolution by eliminating numerical diffusion: The TTLEM 1.0 model. *Earth Surface Dynamics*, *5*(1), 47–66. https://doi.org/10.5194/esurf-5-47-2017

Campforts, B., Vanacker, V., Vanderborght, J., Baken, S., Smolders, E., & Govers, G. (2016). Simulating the mobility of meteoric ^{10}Be in the landscape through a coupled soil-hillslope model (Be2D). *Earth and Planetary Science Letters*, *439*, 143–157. https://doi.org/10.1016/j.epsl.2016.01.017

Caner, L., Radtke, L. M., Vignol-Lelarge, M. L., Inda, A. V., Bortoluzzi, E. C., & Mexias, A. S. (2014). Bacsalt and rhyo-dacite weathering and soil clay formation under subtropical climate in southern Brazil. *Geoderma*, **235–236**, 100–112. https://doi.org/10.1016/j.geoderma.2014.06.024

Catani, F., Segoni, S., & Falorni, G. (2010). An empirical geomorphology-based approach to the spatial prediction of soil thickness at catchment scale. *Water Resources Research*, *46*, W05508. https://doi.org/10.1029/2008WR007450

Chadwick, K. D., & Asner, G. P. (2016). Tropical soil nutrient distributions determined by biotic and hillslope processes. *Biogeochemistry*, *127*(2–3), 273–289. https://doi.org/10.1007/s10533-015-0179-z

Chadwick, O. A., Brimhall, G. H., & Hendricks, D. M. (1990). From a black to a gray box - a mass balance interpretation of pedogenesis. *Geomorphology*, *3*(3–4), 369–390. https://doi.org/10.1016/0169-555X(90)90012-F

Chesworth, W. (2008). In W. Chesworth (Ed.), *Encyclopedia of soil science*. Dordrecht: Springer Netherlands. https://doi.org/10.1007/978-1-4020-3995-9

Chorover, J., Kretzschmar, R., Garcia-Pichel, F., & Sparks, D. L. (2007). Soil biogeochemical processes within the critical zone. *Elements*, *3*(5), 321–326. https://doi.org/10.2113/gselements.3.5.321

Cox, N. J. (1980). On the relationship between bedrock lowering and regolith thickness. *Earth Surface Processes*, *5*(3), 271–274. https://doi.org/10.1002/esp.3760050305

Delvaux, B., Herbillon, A. J., & Vielvoye, L. (1989). Characterization of a weathering sequence of soils derived from volcanic ash in Cameroon. Taxonomic, mineralogical and agronomic implications. *Geoderma*, *45*(3–4), 375–388. https://doi.org/10.1016/0016-7061(89)90017-7

Derose, R. C., Trustrum, N. A., & Blaschke, P. M. (1993). Post-deforestation soil loss from steepland hillslopes in Taranaki, New Zealand. *Earth Surface Processes and Landforms*, *18*(2), 131–144. https://doi.org/10.1002/esp.3290180205

Dixon, J. L., Hartshorn, A. S., Heimsath, A. M., DiBiase, R. A., & Whipple, K. X. (2012). Chemical weathering response to tectonic forcing: A soils perspective from the San Gabriel Mountains, California. *Earth and Planetary Science Letters*, **323–324**, 40–49. https://doi.org/10.1016/j.epsl.2012.01.010

Dixon, J. L., Heimsath, A. M., & Amundson, R. (2009). The critical role of climate and saprolite weathering in landscape evolution. *Earth Surface Processes and Landforms*, *34*(11), 1507–1521. https://doi.org/10.1002/esp.1836

Duzgoren-Aydin, N., Aydin, A., & Malpas, J. (2002). Re-assessment of chemical weathering indices: Case study on pyroclastic rocks of Hong Kong. *Engineering Geology*, *63*(1–2), 99–119. https://doi.org/10.1016/S0013-7952(01)00073-4

Egli, M., Hunt, A. G., Dahms, D., Raab, G., Derungs, C., Raimondi, S., & Yu, F. (2018). Prediction of soil formation as a function of age using the percolation theory approach. *Frontiers in Environmental Science*, *6*(September), 1–21. https://doi.org/10.3389/fenvs.2018.00108

Fedo, C. M., Wayne Nesbitt, H., & Young, G. M. (1995). Unraveling the effects of potassium metasomatism in sedimentary rocks and paleosols, with implications for paleoweathering conditions and provenance. *Geology*, *23*(10), 921. https://doi.org/10.1130/0091-7613(1995)023<0921:UTEOPM>2.3.CO;2

Ferrier, K. L., & Kirchner, J. W. (2008). Effects of physical erosion on chemical denudation rates: A numerical modeling study of soil-mantled hillslopes. *Earth and Planetary Science Letters*, *272*(3-4), 591–599. https://doi.org/10.1016/j.epsl.2008.05.024

Ferrier, K. L., Riebe, C. S., & Jesse Hahm, W. (2016). Testing for supply-limited and kinetic-limited chemical erosion in field measurements of regolith production and chemical depletion. *Geochemistry, Geophysics, Geosystems*, *17*, 2270–2285. https://doi.org/10.1002/2016GC006273

Fiantis, D., Nelson, M., Shamshuddin, J., Goh, T. B., & Van Ranst, E. (2010). Determination of the geochemical weathering indices and trace elements content of new volcanic ash deposits from Mt. Talang (West Sumatra) Indonesia. *Eurasian Soil Science*, *43*(13), 1477–1485. https://doi.org/10.1134/S1064229310130077

Florinsky, I., Eilers, R., Manning, G., & Fuller, L. (2002). Prediction of soil properties by digital terrain modelling. *Environmental Modelling & Software*, *17*(3), 295–311. https://doi.org/10.1016/S1364-8152(01)00067-6

Furbish, D. J., & Fagherazzi, S. (2001). Stability of creeping soil and implications for hillslope evolution. *Water Resources Research*, *37*(10), 2607–2618. https://doi.org/10.1029/2001WR000239

Gabet, E. J. (2007). A theoretical model coupling chemical weathering and physical erosion in landslide-dominated landscapes. *Earth and Planetary Science Letters*, *264*(1–2), 259–265. https://doi.org/10.1016/j.epsl.2007.09.028

Gabet, E. J., & Mudd, S. M. (2009). A theoretical model coupling chemical weathering rates with denudation rates. *Geology*, *37*(2), 151–154. https://doi.org/10.1130/G25270A.1

Gessler, P. E., Chadwick, O. A., Chamran, F., Althouse, L., & Holmes, K. (2000). Modeling soil-landscape and ecosystem properties using terrain attributes. *Soil Science Society of America Journal*, *64*(6), 2046–2056. https://doi.org/10.2136/sssaj2000.6462046x

Gilbert, G. K. (1877). *Report on the geology of the Henry Mountains*. Washington, DC: Government Printing Office.

Gilbert, G. K. (1909). The convexity of hilltops. *The Journal of Geology*, *17*(4), 344–350. https://doi.org/10.1086/621620

Govers, G., Quine, T., & Walling, D. (1993). The effect of water erosion and tillage movement on hillslope profile development: A comparison of field observations and model results. In S. Wicherek (Ed.), *Farm Land Erosion*, (pp. 285–300). Amsterdam: Elsevier.

Govers, G., Vandaele, K., Desmet, P., Poesen, J., & Bunte, K. (1994). The role of tillage in soil redistribution on hillslopes. *European Journal of Soil Science*, *45*(4), 469–478. https://doi.org/10.1111/j.1365-2389.1994.tb00532.x

Green, E., Dietrich, W., & Banfield, J. (2006). Quantification of chemical weathering rates across an actively eroding hillslope. *Earth and Planetary Science Letters*, *242*(1–2), 155–169. https://doi.org/10.1016/j.epsl.2005.11.039

Heimsath, A. M., Dietrich, E. W., Nishiizumi, K., & Finkel, R. C. (1999). Cosmogenic nuclides, topography, and the spatial variation of soil depth. *Geomorphology*, *27*(1–2), 151–172. https://doi.org/10.1016/S0169-555X(98)00095-6

Heimsath, A. M., Dietrich, W. E., Nishiizumi, K., & Finkel, R. C. (1997). The soil production function and landscape equilibrium. *Nature*, *388*(6640), 358–361. https://doi.org/10.1038/41056

Heimsath, A. M., Furbish, D. J., & Dietrich, W. E. (2005). The illusion of diffusion: Field evidence for depth-dependent sediment transport. *Geology*, *33*(12), 949–952. https://doi.org/10.1130/G21868.1

Herbillon, A. J. (1986). Chemical estimation of weatherable minerals present in the diagnostic horizons of low activity clay soils. In F. H. Beinroth, M. N. Camargo, & N. Eswaran (Eds.), *Proceedings of the 8th international Soil Classification Workshop: Classification, Characterization and Utilization of Oxisols (part 1)*, (pp. 39–48). Rio de Janeiro: EMBRAPA.

Hilley, G. E., Chamberlain, C. P., Moon, S., Porder, S., & Willett, S. D. (2010). Competition between erosion and reaction kinetics in controlling silicate-weathering rates. *Earth and Planetary Science Letters*, *293*(1–2), 191–199. https://doi.org/10.1016/j.epsl.2010.01.008

Huang, P. M. (2011). *Handbook of soil sciences* (second edition). Boca Raton: CRC Press. https://doi.org/10.1201/b11267

Humphreys, G. S., & Wilkinson, M. T. (2007). The soil production function: A brief history and its rediscovery. *Geoderma*, *139*(1–2), 73–78. https://doi.org/10.1016/j.geoderma.2007.01.004

Hunt, A. G., & Ghanbarian, B. (2016). Percolation theory for solute transport in porous media: Geochemistry, geomorphology, and carbon cycling. *Water Resources Research*, *52*, 7444–7459. https://doi.org/10.1002/2016WR019289

IUSS Working Group WRB. (2015). World reference base for soil resources 2014, update 2015. International soil classification system for naming soils and creating legends for soil maps. World Soil Resources Reports No. 106. Rome: FAO.

Jahn, R., Blume, H., Asio, V. B., Spaargaren, O., & Schad, P. (2006). *Guidelines for soil description*. Rome: Food and Agricultural Organization.

Jelinski, N. A., Campforts, B., Willenbring, J. K., Schumacher, T. E., Li, S., Lobb, D. A., et al. (2019). Meteoric beryllium-10 as a tracer of erosion due to postsettlement land use in west-central Minnesota, USA. *Journal of Geophysical Research: Earth Surface*, *124*, 874–901. https://doi.org/10.1029/2018JF004720

Johnson, M. O., Mudd, S. M., Pillans, B., Spooner, N. A., Keith Fifield, L., Kirkby, M. J., & Gloor, M. (2014). Quantifying the rate and depth dependence of bioturbation based on optically-stimulated luminescence (OSL) dates and meteoric 10 be. *Earth Surface Processes and Landforms*, *39*(9), 1188–1196. https://doi.org/10.1002/esp.3520

Kirkby, M. (1971). *Hillslope process-response models based on the continuity equation*, *Special Publication*, (Vol. 3, pp. 5–30). Hoboken, NJ, USA: Institute of British Geographers.

Lebedeva, M. I., Fletcher, R. C., & Brantley, S. L. (2010). A mathematical model for steady-state regolith production at constant erosion rate. *Earth Surface Processes and Landforms*, *35*(5), 508–524. https://doi.org/10.1002/esp.1954

Lebedeva, M. I., & Brantley, S. L. (2013). Exploring geochemical controls on weathering and erosion of convex hillslopes: Beyond the empirical regolith production function. *Earth Surface Processes and Landforms*, *38*(15), 1793–1807. https://doi.org/10.1002/esp.3424

Lopes, F. (2006). Utilização do Modelo Century para avaliar a dinâmica do Carbono do solo em uma pequena bacia hidrográfica rural. Universidade Federal do Rio Grande Do Sul.

Maher, K. (2010). The dependence of chemical weathering rates on fluid residence time. *Earth and Planetary Science Letters*, *294*(1–2), 101–110. https://doi.org/10.1016/j.epsl.2010.03.010

Maher, K., & Navarre-Sitchler, A. (2019). Reactive transport processes that drive chemical weathering: From making space for water to dismantling continents. *Reviews in Mineralogy and Geochemistry*, *85*(1), 349–380. https://doi.org/10.2138/rmg.2018.85.12

Mehnatkesh, A., Ayoubi, S., Jalalian, A., & Sahrawat, K. L. (2013). Relationships between soil depth and terrain attributes in a semi arid hilly region in western Iran. *Journal of Mountain Science*, *10*(1), 163–172. https://doi.org/10.1007/s11629-013-2427-9

Merritts, D. J., Chadwick, O. A., & Hendricks, D. M. (1991). Rates and processes of soil evolution on uplifted marine terraces, northern California. *Geoderma*, *51*(1–4), 241–275. https://doi.org/10.1016/0016-7061(91)90073-3

Merten, G. H., Minella, J. P. G., Moro, M., Maier, C., Cassol, E. A., Walling, D. E., et al. (2010). The effects of soil conservation on sediment yield and sediment source dynamics in a catchment in southern Brazil. In K. Banasik (Ed.), *Sediment Dynamics for a Changing Future*, IAHS Publication, (Vol. *337*, pp. 59–67). Wallingford, UK: IAHS Press.

Minasny, B., & McBratney, A. B. (2001). A rudimentary mechanistic model for soil formation and landscape development. *Geoderma*, *103*(1–2), 161–179. https://doi.org/10.1016/S0016-7061(01)00075-1

Minasny, B., & McBratney, A. B. (2006). Mechanistic soil–landscape modelling as an approach to developing pedogenetic classifications. *Geoderma*, *133*(1–2), 138–149. https://doi.org/10.1016/j.geoderma.2006.03.042

Minasny, B., McBratney, A. B., & Salvador-Blanes, S. (2008). Quantitative models for pedogenesis—A review. *Geoderma*, *144*(1–2), 140–157. https://doi.org/10.1016/j.geoderma.2007.12.013

Minella, J. P. G., Merten, G. H., Walling, D. E., & Reichert, J. M. (2009). Changing sediment yield as an indicator of improved soil management practices in southern Brazil. *Catena*, *79*(3), 228–236. https://doi.org/10.1016/j.catena.2009.02.020

Minella, J. P. G., Merten, G. H., Reichert, J. M., & Clarke, R. T. (2008). Estimating suspended sediment concentrations from turbidity measurements and the calibration problem. *Hydrological Processes*, *22*(12), 1819–1830. https://doi.org/10.1002/hyp.6763

Minella, J. P. G., Walling, D. E., & Merten, G. H. (2014). Establishing a sediment budget for a small agricultural catchment in southern Brazil, to support the development of effective sediment management strategies. *Journal of Hydrology*, *519*, 2189–2201. https://doi.org/10.1016/j.jhydrol.2014.10.013

Mohanty, B., Gupta, A., & Das, B. S. (2016). Estimation of weathering indices using spectral reflectance over visible to mid-infrared region. *Geoderma*, *266*, 111–119. https://doi.org/10.1016/j.geoderma.2015.11.030

Molina, A., Vanacker, V., Corre, M. D., & Veldkamp, E. (2019). Patterns in soil chemical weathering related to topographic gradients and vegetation structure in a high Andean tropical ecosystem. *Journal of Geophysical Research: Earth Surface*, *124*, 666–685. https://doi.org/10.1029/2018JF004856

Morellato, L. P. C., & Haddad, C. F. B. (2000). Introduction: The Brazilian Atlantic forest. *Boitropica*, *32*(4b), 786–792. https://www.jstor.org/stable/2663917

Moriasi, D. N., Arnold, J. G., Van Liew, M. W., Bingner, R. L., Harmel, R. D., & Veith, T. L. (2007). Model evaluation guidelines for systematic quantification of accuracy in watershed simulations. *Transactions of the ASABE*, *50*(3), 885–900. https://doi.org/10.13031/2013.23153

Mudd, S. M., Yoo, K., & Weinman, B. (2014). Quantifying geomorphic controls on time in weathering systems. *Procedia Earth and Planetary Science*, *10*, 249–253. https://doi.org/10.1016/j.proeps.2014.08.033

Mudd, S. M., & Furbish, D. J. (2006). Using chemical tracers in hillslope soils to estimate the importance of chemical denudation under conditions of downslope sediment transport. *Journal of Geophysical Research*, *111*, F02021. https://doi.org/10.1029/2005JF000343

Mudd, S. M., & Yoo, K. (2010). Reservoir theory for studying the geochemical evolution of soils. *Journal of Geophysical Research*, *115*, F03030. https://doi.org/10.1029/2009JF001591

Nash, J. E., & Sutcliffe, J. V. (1970). River flow forecasting through conceptual models part I—A discussion of principles. *Journal of Hydrology*, *10*(3), 282–290. https://doi.org/10.1016/0022-1694(70)90255-6

Nesbitt, H. W., & Young, G. M. (1982). Early Proterozoic climates and plate motions inferred from major element chemistry of lutites. *Nature*, *299*(5885), 715–717. https://doi.org/10.1038/299715a0

Nesbitt, H. W., & Young, G. M. (1989). Formation and diagenesis of weathering profiles. *The Journal of Geology*, *97*(2), 129–147. https://doi.org/10.1086/629290

Nezat, C. A., Blum, J. D., Klaue, A., Johnson, C. E., & Siccama, T. G. (2004). Influence of landscape position and vegetation on long-term weathering rates at the Hubbard Brook experimental forest, New Hampshire, USA. *Geochimica et Cosmochimica Acta*, *68*(14), 3065–3078. https://doi.org/10.1016/j.gca.2004.01.021

Nocita, M., Stevens, A., van Wesemael, B., Aitkenhead, M., Bachmann, M., Barth, B., et al. (2015). Soil spectroscopy: An alternative to wet chemistry for soil monitoring. *Advances in Agronomy*, *132*, 139–159. https://doi.org/10.1016/bs.agron.2015.02.002

Opolot, E., Yu, Y. Y., & Finke, P. A. (2015). Modeling soil genesis at pedon and landscape scales: Achievements and problems. *Quaternary International*, *376*, 34–46. https://doi.org/10.1016/j.quaint.2014.02.017

Osat, M., Heidari, A., Karimian Eghbal, M., & Mahmoodi, S. (2016). Impacts of topographic attributes on soil taxonomic classes and weathering indices in a hilly landscape in Northern Iran. *Geoderma*, *281*, 90–101. https://doi.org/10.1016/j.geoderma.2016.06.020

Peel, M. C., Finlayson, B. L., & McMahon, T. A. (2007). Updated world map of the Koppen-Geiger climate classification. *Hydrology and Earth System Sciences*, *11*(5), 1633–1644. https://doi.org/10.5194/hess-11-1633-2007

Pelckmans, I. (2018). Summary for policymakers. In Intergovernmental Panel on Climate Change (Ed.), *Climate change 2013—The physical science basis*, (pp. 1–30). Cambridge: Cambridge University Press. https://doi.org/10.1017/CBO9781107415324.004

Pelletier, J. D., & Rasmussen, C. (2009). Geomorphically based predictive mapping of soil thickness in upland watersheds. *Water Resources Research*, *45*, WO9417. https://doi.org/10.1029/2008WR007319

Pillar, V. D. P., & Quadros, F. (1999). Grassland-forest boundaries in Southern Brazil. In *Conference on recent shifts in vegetation boundaries of deciduous forests, especially due to general global warming*, (Vol. 12, pp. 301–316). Basel: Birkhäuser Basel. https://doi.org/10.1007/978-3-0348-8722-9_17

Price, J. R., & Velbel, M. A. (2003). Chemical weathering indices applied to weathering profiles developed on heterogeneous felsic metamorphic parent rocks. *Chemical Geology*, *202*(3–4), 397–416. https://doi.org/10.1016/j.chemgeo.2002.11.001

Rasmussen, C., Dahlgren, R. A., & Southard, R. J. (2010). Basalt weathering and pedogenesis across an environmental gradient in the southern Cascade Range, California, USA. *Geoderma*, *154*(3–4), 473–485. https://doi.org/10.1016/j.geoderma.2009.05.019

Rasmussen, C., & Tabor, N. J. (2007). Applying a quantitative pedogenic energy model across a range of environmental gradients. *Soil Science Society of America Journal*, *71*(6), 1719–1729. https://doi.org/10.2136/sssaj2007.0051

Reaney, S. M. (2003). Modelling runoff generation and connectivity for semi-arid hillslopes and small catchments. University of Leeds. Retrieved from http://etheses.whiterose.ac.uk/id/eprint/720

Renne, P. R., Ernesto, M., Pacca, I. G., Coe, R. S., Glen, J. M., Prevot, M., & Perrin, M. (1992). The age of Parana flood volcanism, rifting of Gondwanaland, and the Jurassic-Cretaceous boundary. *Science*, *258*(5084), 975–979. https://doi.org/10.1126/science.258.5084.975

Richter, N., Jarmer, T., Chabrillat, S., Oyonarte, C., Hostert, P., & Kaufmann, H. (2009). Free Iron oxide determination in Mediterranean soils using diffuse reflectance spectroscopy. *Soil Science Society of America Journal*, *73*(1), 72–81. https://doi.org/10.2136/sssaj2008.0025

Riebe, C. S., Hahm, W. J., & Brantley, S. L. (2017). Controls on deep critical zone architecture: A historical review and four testable hypotheses. *Earth Surface Processes and Landforms*, *42*(1), 128–156. https://doi.org/10.1002/esp.4052

Riebe, C. S., Kirchner, J. W., & Finkel, R. C. (2003). Long-term rates of chemical weathering and physical erosion from cosmogenic nuclides and geochemical mass balance. *Geochimica et Cosmochimica Acta*, *67*(22), 4411–4427. https://doi.org/10.1016/S0016-7037(03)00382-X

Riebe, C. S., Kirchner, J. W., & Finkel, R. C. (2004). Sharp decrease in long-term chemical weathering rates along an altitudinal transect. *Earth and Planetary Science Letters*, *218*(3–4), 421–434. https://doi.org/10.1016/S0012-821X(03)00673-3

Riebe, C. S., Kirchner, J. W., Granger, D. E., & Finkel, R. C. (2001). Strong tectonic and weak climatic control of long-term chemical weathering rates. *Geology*, *29*(6), 511–514. https://doi.org/10.1130/0091-7613(2001)029<0511:STAWCC>2.0.CO;2

Robinet, J., Minella, J. P. G., de Barros, C. A. P., Schlesner, A., Lücke, A., Ameijeiras-Mariño, Y., et al. (2018). Impacts of forest conversion to arable land and agriculture practices on the water pathways in southern Brazil. *Hydrological Processes*, *32*(15), 2304–2317. https://doi.org/10.1002/hyp.13155

Robinet, J., von Hebel, C., Govers, G., van der Kruk, J., Minella, J. P. G., Schlesner, A., et al. (2018). Spatial variability of soil water content and soil electrical conductivity across scales derived from electromagnetic induction and time domain reflectometry. *Geoderma*, *314*, 160–174. https://doi.org/10.1016/j.geoderma.2017.10.045

Roering, J. J., Kirchner, J. W., & Dietrich, W. E. (1999). Evidence for nonlinear, diffusive sediment transport on hillslopes and implications for landscape morphology. *Water Resources Research*, *35*(3), 853–870. https://doi.org/10.1029/1998WR900090

Saco, P. M., Willgoose, G. R., & Hancock, G. R. (2006). Spatial organization of soil depths using a landform evolution model. *Journal of Geophysical Research*, *111*, F02016. https://doi.org/10.1029/2005JF000351

Schoonejans, J., Vanacker, V., Opfergelt, S., & Christl, M. (2017). Long-term soil erosion derived from in-situ ^{10}Be and inventories of meteoric ^{10}Be in deeply weathered soils in southern Brazil. *Chemical Geology*, *466*, 380–388. https://doi.org/10.1016/j.chemgeo.2017.06.025

Schoonejans, Jérôme. (2016). Constraining soil formation and development through quantitative analyses of chemical weathering and physical erosion. Université catholoque de Louvain.

Schoonejans, J., Vanacker, V., Opfergelt, S., Ameijeiras-Mariño, Y., & Christl, M. (2016). Kinetically limited weathering at low denudation rates in semiarid climatic conditions. *Journal of Geophysical Research: Earth Surface*, *121*, 336–350. https://doi.org/10.1002/2015JF003626

Shobe, C. M., Tucker, G. E., & Barnhart, K. R. (2017). The SPACE 1.0 model: A Landlab component for 2-D calculation of sediment transport, bedrock erosion, and landscape evolution. *Geoscientific Model Development*, *10*(12), 4577–4604. https://doi.org/10.5194/gmd-10-4577-2017

Small, E. E., Anderson, R. S., & Hancock, G. S. (1999). Estimates of the rate of regolith production using and from an alpine hillslope. *Geomorphology*, *27*(1–2), 131–150. https://doi.org/10.1016/S0169-555X(98)00094-4

Soriano-Disla, J. M., Janik, L. J., Viscarra Rossel, R. A., Macdonald, L. M., & McLaughlin, M. J. (2014). The performance of visible, near-, and mid-infrared reflectance spectroscopy for prediction of soil physical, chemical, and biological properties. *Applied Spectroscopy Reviews*, *49*(2), 139–186. https://doi.org/10.1080/05704928.2013.811081

The MathWorks, I. (2020). How the genetic algorithm works. Retrieved February 27, 2020, from https://www.mathworks.com/help/gads/how-the-genetic-algorithm-works.html

Thompson, J. A., Pena-Yewtukhiw, E. M., & Grove, J. H. (2006). Soil–landscape modeling across a physiographic region: Topographic patterns and model transportability. *Geoderma*, *133*(1–2), 57–70. https://doi.org/10.1016/j.geoderma.2006.03.037

Tsai, C. C., Chen, Z. S., Duh, C. T., & Horng, F. W. (2001). Prediction of soil depth using a soil-landscape regression model: A case study on forest soils in southern Taiwan. *Proceedings of the National Science Council, Republic of China. Part B, Life Sciences*, *25*(1), 34–39.

Tsui, C., Chen, Z., & Hsieh, C. (2004). Relationships between soil properties and slope position in a lowland rain forest of southern Taiwan. *Geoderma*, *123*(1–2), 131–142. https://doi.org/10.1016/j.geoderma.2004.01.031

Tucker, G. E., & Bradley, D. N. (2010). Trouble with diffusion: Reassessing hillslope erosion laws with a particle-based model. *Journal of Geophysical Research*, F00A10. https://doi.org/10.1029/2009jf001264

Turner, S., Regelous, M., Kelley, S., Hawkesworth, C., & Mantovani, M. (1994). Magmatism and continental break-up in the South Atlantic: High precision ^{40}Ar-^{39}Ar geochronology. *Earth and Planetary Science Letters*, *121*(3–4), 333–348. https://doi.org/10.1016/0012-821X(94)90076-0

Van de Broek, M., & Govers, G. (2019). Quantification of organic carbon concentrations and stocks of tidal marsh sediments via mid-infrared spectroscopy. *Geoderma*, *337*, 555–564. https://doi.org/10.1016/j.geoderma.2018.09.051

Van Oost, K., Van Muysen, W., Govers, G., Heckrath, G., Quine, T. A., & Poesen, J. (2003). Simulation of the redistribution of soil by tillage on complex topographies. *European Journal of Soil Science*, *54*(1), 63–76. https://doi.org/10.1046/j.1365-2389.2003.00470.x

Vanacker, V., Ameijeiras-Mariño, Y., Schoonejans, J., Cornélis, J., Minella, J. P. G., Lamouline, F., et al. (2019). Land use impacts on soil erosion and rejuvenation in southern Brazil. *Catena*, *178*(March), 256–266. https://doi.org/10.1016/j.catena.2019.03.024

Vieira, B. C., Salgado, A. A. R., & Santos, L. J. C. (2015). In B. C. Vieira, A. A. R. Salgado, & L. J. C. Santos (Eds.), *Landscapes and landforms of Brazil*. Dordrecht: Springer Netherlands. https://doi.org/10.1007/978-94-017-8023-0

Viscarra Rossel, R. A., Walvoort, D. J. J., McBratney, A. B., Janik, L. J., & Skjemstad, J. O. (2006). Visible, near infrared, mid infrared or combined diffuse reflectance spectroscopy for simultaneous assessment of various soil properties. *Geoderma*, *131*(1–2), 59–75. https://doi.org/10.1016/j.geoderma.2005.03.007

Vohland, M., Ludwig, M., Thiele-Bruhn, S., & Ludwig, B. (2014). Determination of soil properties with visible to near- and mid-infrared spectroscopy: Effects of spectral variable selection. *Geoderma*, **223–225**(1), 88–96. https://doi.org/10.1016/j.geoderma.2014.01.013

Wackett, A. A., Yoo, K., Amundson, R., Heimsath, A. M., & Jelinski, N. A. (2018). Climate controls on coupled processes of chemical weathering, bioturbation, and sediment transport across hillslopes. *Earth Surface Processes and Landforms*, *43*(8), 1575–1590. https://doi.org/10.1002/esp.4337

White, A. F., Blum, A. E., Schulz, M. S., Bullen, T. D., Harden, J. W., & Peterson, M. L. (1996). Chemical weathering of a soil chronosequence on granite alluvium I. Reaction rates based on changes in soil mineralogy. *Geochimica et Cosmochimica Acta*, *60*(14), 2533–2550.

White, A. F., Blum, A. E., Schulz, M. S., Vivit, D. V., Stonestrom, D. A., Larsen, M., et al. (1998). Chemical weathering in a tropical watershed, Luquillo Mountains, Puerto Rico: I. Long-term versus short-term weathering fluxes. *Geochimica et Cosmochimica Acta*, *62*(2), 209–226. https://doi.org/10.1016/S0016-7037(97)00335-9

White, A. F., & Brantley, S. L. (2003). The effect of time on the weathering of silicate minerals: Why do weathering rates differ in the laboratory and field? *Chemical Geology*, *202*(3–4), 479–506. https://doi.org/10.1016/j.chemgeo.2003.03.001

Wyshnytzky, C. E., Ouimet, W. B., McCarthy, J., Dethier, D. P., Shroba, R. R., Bierman, P. R., & Rood, D. H. (2015). Meteoric ^{10}Be, clay, and extractable iron depth profiles in the Colorado Front Range: Implications for understanding soil mixing and erosion. *Catena*, *127*, 32–45. https://doi.org/10.1016/j.catena.2014.12.008

Yoo, K., Amundson, R., Heimsath, A. M., Dietrich, W. E., & Brimhall, G. H. (2007). Integration of geochemical mass balance with sediment transport to calculate rates of soil chemical weathering and transport on hillslopes. *Journal of Geophysical Research*, *112*, F02013. https://doi.org/10.1029/2005JF000402

Yoo, K., & Mudd, S. M. (2008). Toward process-based modeling of geochemical soil formation across diverse landforms: A new mathematical framework. *Geoderma*, *146*(1–2), 248–260. https://doi.org/10.1016/j.geoderma.2008.05.029

Yoo, K., Mudd, S. M., Sanderman, J., Amundson, R., & Blum, A. (2009). Spatial patterns and controls of soil chemical weathering rates along a transient hillslope. *Earth and Planetary Science Letters*, *288*(1–2), 184–193. https://doi.org/10.1016/j.epsl.2009.09.021

References From the Supporting Information

Akaike, H. (1987). Factor analysis and AIC. *Psychometrika*, *52*(3), 317–332. https://doi.org/10.1007/BF02294359

Bayer, A., Bachmann, M., Müller, A., & Kaufmann, H. (2012). A comparison of feature-based MLR and PLS regression techniques for the prediction of three soil constituents in a degraded South African ecosystem. *Applied and Environmental Soil Science*, *2012*, 971252. https://doi.org/10.1155/2012/971252

BELSPO. (2017). SOils under GLObal change. Project Rationale. Retrieved from https://hal.elic.ucl.ac.be/soglo/project.html

Chao, T. T., & Sanzolone, R. F. (1992). Decomposition techniques. *Journal of Geochemical Exploration*, *44*(1–3), 65–106. https://doi.org/10.1016/0375-6742(92)90048-D

Cozzolino, D., & Morón, A. (2003). The potential of near-infrared reflectance spectroscopy to analyse soil chemical and physical characteristics. *Journal of Agricultural Science*, *140*(1), 65–71. https://doi.org/10.1017/S0021859602002836

Demattê, J. A. M., & da Silva Terra, F. (2014). Spectral pedology: A new perspective on evaluation of soils along pedogenetic alterations. *Geoderma*, **217–218**, 190–200. https://doi.org/10.1016/j.geoderma.2013.11.012

Kohler, A., Kirschner, C., Oust, A., & Martens, H. (2005). Extended multiplicative signal correction as a tool for separation and characterization of physical and chemical information in Fourier transform infrared microscopy images of cryo-sections of beef loin. *Applied Spectroscopy*, *59*(6), 707–716. https://doi.org/10.1366/0003702054280649

Mehra, O. P. (1958). Iron oxide removal from soils and clays by a dithionite-citrate system buffered with sodium bicarbonate. *Clays and Clay Minerals*, *7*(1), 317–327. https://doi.org/10.1346/ccmn.1958.0070122

Peltre, C., Bruun, S., Du, C., Thomsen, I. K., & Jensen, L. S. (2014). Assessing soil constituents and labile soil organic carbon by mid-infrared photoacoustic spectroscopy. *Soil Biology and Biochemistry*, *77*, 41–50. https://doi.org/10.1016/j.soilbio.2014.06.022

Varmuza, K., & Filzmoser, P. (2009). *Introduction to multivariate statistical analysis in chemometrics*. Boca Raton: Taylor & Francis Group.

Xie, X.-L., Pan, X.-Z., & Sun, B. (2012). Visible and near-infrared diffuse reflectance spectroscopy for prediction of soil properties near a copper smelter. *Pedosphere*, *22*(3), 351–366. https://doi.org/10.1016/S1002-0160(12)60022-8